

**Lorentz force sismometry: a novel technique to
measure the electrical conductivity of solid and
fluid metals**

DISSERTATION

zur Erlangung des akademischen Grades

DOKTORINGENIEUR

(Dr.-Ing.)

vorgelegt der

Fakultät für Maschinenbau der

Technischen Universität Ilmenau

von Frau

M.Sc. SHATHA ALKHALIL

geboren am 15.09.1984 in Homs, Syrien

Tag der Einreichung: 27.11.2015

Tag der wissenschaftlichen Aussprache: 25.02.2016

Gutachter: 1. Univ.-Prof. Dr. André Thess
 2. Univ.-Prof. Dr. Thomas Fröhlich
 3. Prof. Dr. Donald R. Sadoway

Zusammenfassung

Lorentzkraft Sigmometrie, "LOFOS," ist eine neuartige Technik zur Messung unterschiedlicher physikalischer Eigenschaften von Flüssigmetall, wie der elektrischen Leitfähigkeit, Viskosität oder Dichte. Der Fokus dieser Arbeit liegt auf der Messung der elektrischen Leitfähigkeit von festen und flüssigen Metallen mit dem sogenannten mobilen LOFOS.

Diese Technik basiert auf den Grundsätzen der Magnetohydrodynamik: Durch die Bewegung eines elektrischen Leiters in einem von außen angelegtem Magnetfeld werden Wirbelströme innerhalb des Leiters induziert. Nach dem Ampereschen Gesetz erzeugen diese Wirbelströme wiederum ein sekundäres Magnetfeld. Durch Wechselwirkung zwischen den Wirbelströmen und dem magnetischen Gesamtfeld entstehen Lorentzkräfte, die den Fluss abschwächen. Nach Newtons drittem Gesetz (*actio und reactio*) wirken die Lorentzkräfte auch auf den Magneten mit gleichem Betrag, aber in entgegengesetzter Richtung [Thess *et al.*, 2007]. Diese Kraft kann gemessen werden und ist proportional zu der elektrischen Leitfähigkeit des flüssigen oder festen Leiters. Diese Tatsache wird für die kontaktlose Geschwindigkeitsmessung "Lorentz force velocimetry" und für die Erkennung von Defekten in Festkörpern "Lorentz force eddy current testing" genutzt.

Ziel dieser Arbeit ist es zu testen und zu zeigen, dass LOFOS erfolgreich die elektrische Leitfähigkeit von festen und flüssigen Metallen messen kann. Mehrere Experimente wurden durchgeführt um dieses zu zeigen, beginnend mit festen Zylindern aus Kupfer, Aluminium und Messing, die eine Länge von 300 mm und einem Durchmesser von 10 mm haben. Die ersten Experimente wurden an festen Metallen mit bekannter elektrischer Leitfähigkeit durchgeführt (Aluminium und Kupfer), um den Kalibrierungsfaktor zu ermitteln. Dieser Kalibrierungsfaktor wurde dann benutzt um die Leitfähigkeit eines Zylinders aus Messing zu messen. Die Anordnung von LOFOS für die Messung an festen Metallen bedarf einiger technischer Veränderungen im Vergleich zu der Messung an Fluiden. Diese Veränderungen sind nötig um die Zeit der Wechselwirkung zwischen festen Metallen und externen magnetischen Feld, welches durch einen Halbach Zylinder Magneten erzeugt wird, zu verlängern [Alkhalil *et al.*, 2015].

Die zweite Reihe an Experimenten erfolgte mit Flüssigmetall. Zu Beginn wurde die Legierung $\text{Ga}^{67}\text{In}^{20.5}\text{Sn}^{12.5}$ verwendet, deren physikalische Eigenschaften bekannt sind. Diese eutektische Legierung hat einen Schmelzpunkt von $T_m = 10.5^\circ\text{C}$ und ist daher flüssig bei Raumtemperatur, wohingegen die zweiten Versuche

mit flüssigem Zinn durchgeführt wurden, welches einen Schmelzpunkt von $T_m = 232\text{ °C}$ hat. Für die Strömungsmessungen fertigten wir einen speziellen kegelförmigen Behälter aus Quarz an, welcher Temperaturen von Raumtemperatur bis zu 1000 °C aushält. Die Düse hat einen Durchmesser von 8 mm und ermöglicht den Durchfluss von flüssigem Metall durch das Magnetsystem in $\Delta t \approx 5\text{ s}$, was notwendig für die Messung der Lorentzkraft mit hoher Genauigkeit ist. Um das LOFOS Lorentzkraft Messsystem vor hohen Temperaturen zu schützen, haben wir eine externe Luftkompressor Pumpe hinzugefügt.

Beide Experimente bestätigen, dass Lorentzkraft Sigmometrie die elektrische Leitfähigkeit von festen und flüssigen Metall ermitteln kann. Der Fehler für die Messungen an festen Metallen beträgt bis zu 6.5% , für die Messungen an flüssigen Metal bis zu 10% .

Abstract

Lorentz force sigmometry, "LOFOS," is a novel technique with three different configuration setups for measuring different physical properties of molten metals such as electrical conductivity, viscosity, and density . However, this thesis focuses on measuring the electrical conductivity of the solid and molten metals using the so-called mobile LOFOS setup.

The interaction of an electrically conducting fluid with an externally applied magnetic field leads to a force that acts upon the magnetic field generating system and drags it along the flow direction [Thess *et al.*, 2007]. This force linearly depends on the electrical conductivity of the conducting fluid and can be measured using force sensors. The aim of this study was to test and successfully prove that LOFOS can measure the electrical conductivity of solid and molten metals. Several experiments were performed to achieve this goal, starting with experiments using three solid cylindrical bars made of copper, aluminum, and brass 300 mm in length and 10 mm in diameter. The first series of experiments were carried out with known electrically conductive metals, aluminum and copper, in order to compute the calibration factor of the device. We then used the same calibration factor to estimate the unknown electrical conductivity of a brass bar [Alkhalil *et al.*, 2015]. The setup of LOFOS for solid measurements required some technical changes as compared to the one for fluid measurements. This modification was necessary to extend the interaction time between the solid bar and the external magnetic field generated by a Halbach cylinder magnet.

The second series of experiments were with molten metals. The first series with known physical properties alloy having the composition of $\text{Ga}^{67}\text{In}^{20.5}\text{Sn}^{12.5}$. This is a eutectic alloy at room temperature, and its melting temperature is $T_m = 10.5^\circ\text{C}$, whereas the second series was carried out with high-temperature molten tin at $T_m = 232^\circ\text{C}$. For fluid measurements, we fabricated a special quartz conical vessel able to withstand temperatures ranging from room temperature up to 1000°C . The nozzle had a diameter of 8 mm, and it allowed the flow of molten metal across the magnet system during some seconds, which is reasonable for measuring the Lorentz force with good accuracy. In order to protect the LOFOS force measurement system from high temperatures, we added an external air compressor pump to the LOFOS setup.

Both experiments with solid and molten metals prove that Lorentz force sigmometry is able to measure the electrical conductivity of solid and molten metals. The uncertainty of solid measurements is in total up to 5% , while for molten metals measurements is less than 10% .

Contents

Zusammenfassung	i
Abstract	iii
Contents	v
1 Introduction	1
1.1 Motivation	1
1.2 Objective and overview of this thesis	4
2 State of the art	7
2.1 State of the art of electrical conductivity of solid metals	7
2.1.1 Two-probe method for measuring the electrical conductivity of solid metals	8
2.1.2 Four-probe method for measuring the electrical conductivity of solid metals	9
2.1.3 Bridge methods [direct current (DC) and alternating current (AC)]	11
2.1.4 Eddy current method	12
2.2 State of the art of electrical conductivity of fluid metals	16
2.2.1 Contact measurements	16
2.2.2 Containerless and Contactless Measurements	17
2.2.3 Contactless inductive measurements	20
3 Fundamentals and Experimental Setup	23
3.1 Fundamentals	23
3.2 Experimental setup for fluid measurements	25
3.3 Experimental setup for solid measurements	27
3.4 Halbach cylinder magnet	29
3.5 Force measurement system	35
3.6 Calibration of Lorentz force sigmometry device	38
3.7 Uncertainties analysis	40
4 Electrical conductivity measurements of solid metals	43
4.1 First test of the device / short solid bars measurements	43
4.2 Measurement procedure with long solid bars	46
4.3 Determination of calibration factor using copper and aluminum bars	48

CONTENTS

4.3.1	Copper measurements	49
4.3.2	Aluminum measurements	51
4.4	Electrical conductivity measurement of brass bar	54
5	Electrical conductivity measurements of molten metals	59
5.1	Calibration factor calculation using eutectic alloy GaInSn	59
5.1.1	Measurements procedure	60
5.1.2	Lorentz force signal of galinstan alloy	62
5.2	Electrical conductivity measurement of molten tin	65
6	Conclusion and Outlook	75
	Appendix	79
6.1	Physical properties of galinstan alloy	79
6.2	Data sheet of strain gauge sensor	80
	List of Figures	83
	References	91
	Acknowledgements	95
	Erklärung	97

Chapter 1

Introduction

1.1 Motivation

Metallurgical processes such as continuous casting [Blair & Stevens, 1995] and powder production (see Fig. 1.1) were proposed as early as the mid-1800s. The extensive industrial application of these processes started in the late 1960s and early 1970s. Currently, as an example, the continuous casting ratio of crude steel output is approximately 90%. In spite of this growth, however, the quality of the finished products and efficiency of these processes are still not sufficient. For precise control of the production process in industry, the following is needed:

- First, precise knowledge of the physical properties of molten metals (such as electrical conductivity, density, viscosity, and surface tension) is crucial for the proper optimization and control over the metallurgical processes. Until today, these factors have been known in metallurgy with an uncertainty higher than 10%. Among all these properties, the electrical conductivity is of particular interest because it helps in determining the local skin depth of metal melts, which determines the energy efficiency in the electromagnetic processing of materials, including electromagnetic stirring [Sivak *et al.*, 2009]. It also helps us draw inferences about the electronic transport properties and the structural heterogeneity of the metal [Brodova *et al.*, 2002].
- Second, flow rate measurements of liquid metal at several locations is desirable because the quality of the final product of a metallurgical process strongly depends on the quantity of individual alloy components involved

in the production process. This task remains challenging. Because molten melts in metallurgy are hot and aggressive and because the wetting characteristics between the melt and the probe are mostly unknown, contact methods for flow measurements such as mechanical flow meters, pressure-based flow meters, thermal flow meters, and electromagnetic flow meters cannot be applied [Baker, 2000; Jensen, 2004; Shercliff, 1962]. Thus, non-contact measurement techniques are of interest. However, because liquid metals have high opacity, optical measurement systems such as laser Doppler anemometry and particle image velocimetry cannot be applied. On the other hand, liquid metals are excellent electrical conductors, and so electromagnetic measurement techniques are promising candidates to meet the challenge. Among these candidates, flow meters based on the measurement of (i) flow-induced Lorentz forces [Thess *et al.*, 2006], [Kolesnikov *et al.*, 2011] that act as a braking force on the flow but also as a counteracting pulling force on an externally arranged magnet system and (ii) flow-induced phase shifts [Priede *et al.*, 2011] of electrical fields between a submitting coil and two receiving coils have been developed and already successfully applied under industrial conditions. However, these methods require precise knowledge of the electrical conductivity of the melt in order to evaluate the melt velocity from the measured data.

From the above discussion, we notice that accurate measurements of the electrical conductivity of molten metals is important for improving the current metallurgical process and thus the quality of the finished product.

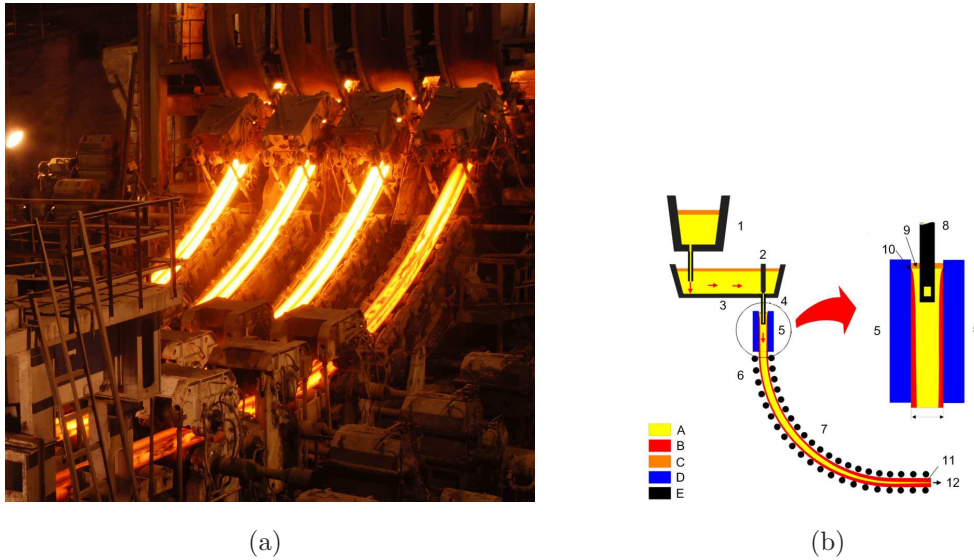


Figure 1.1: Continuous casting process of steel. (a) Manufacturing process of continuous casting of steel in industry (courtesy of Vizag Steel). (b) Continuous casting process. 1: Ladle. 2: Stopper. 3: Tundish. 4: Shroud. 5: Mold. 6: Roll support. 7: Turning zone. 8: Shroud. 9: Bath level. 10: Meniscus. 11: Withdrawal unit. 12: Slab. A: Liquid metal. B: Solidified metal. C: Slag. D: Water-cooled copper plates. E: Refractory material (courtesy of Wikipedia).

In the present thesis, we address the problem of non-contact measurement of the electrical conductivity of liquid metals in order to support the flow measurement techniques described above, which need this melt property as an input quantity. We term the method “Lorentz force sigmometry,” where the term “sigmometry” refers to the letter sigma, σ , which is often used to denote the electrical conductivity. The Lorentz force sigmometry method is based on the phenomenon of eddy current generation in a moving conductor exposed to a magnetic field (see Fig. 1.2). Based on Ampere’s law, the eddy currents in turn generate a secondary magnetic field; as a result of the interaction between eddy currents and the magnetic fields, the Lorentz force is generated. This force acts as a brake on the conductor. Owing to Newton’s third law (the law of action-reaction), a force that is equal to the Lorentz force and is directly proportional to the electrical conductivity of the conductive fluid or solid acts on the magnet. We can measure this force using a force sensor located beneath the magnet. This phenomenon has been used in contactless velocity measurements in the form of “Lorentz force velocimetry” (LFV) and for detecting defects in a solid bar in the form of “Lorentz force eddy current testing” (LET).

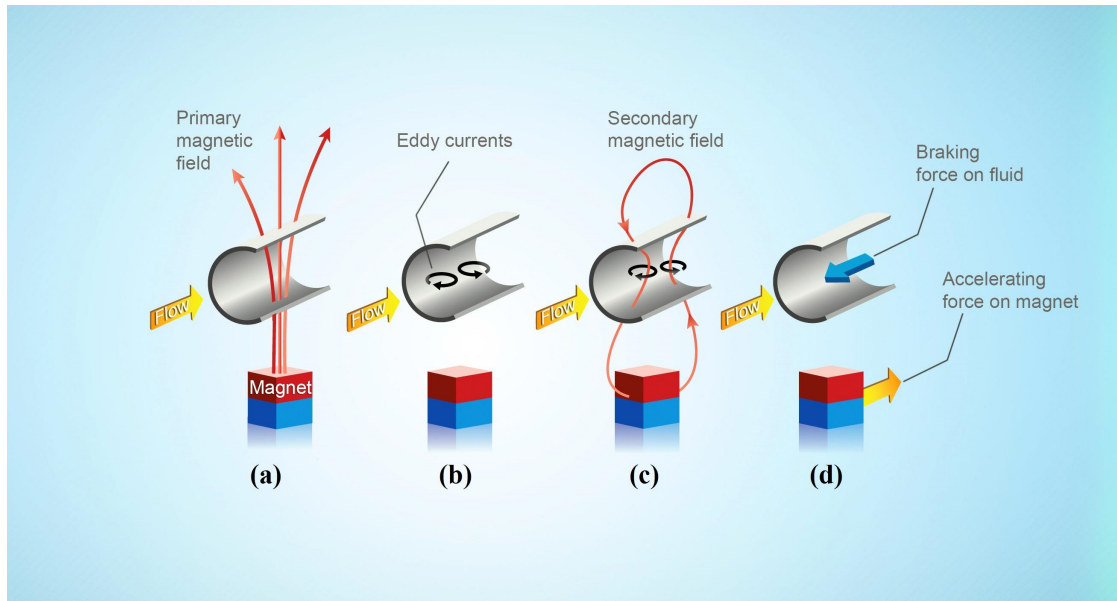


Figure 1.2: Schematic of the working principle of Lorentz force velocimetry. (a) A moving electrically conductive fluid is exposed to a magnetic field. (b) An eddy current is induced inside the fluid by the external magnetic field. (c) The eddy current induces a secondary magnetic field. (d) The interaction of the magnetic field with the eddy current generates a Lorentz force (braking force) on the fluid. Then, owing to Newton's third law, a force equal to the Lorentz force acts on the magnet, which can be measured using a force sensor.

1.2 Objective and overview of this thesis

Lorentz force velocimetry with its simple concept can measure three important physical properties—electrical conductivity, density, and viscosity—using three different configurations. However, in this study, we aim to prove experimentally that Lorentz force velocimetry can measure the electrical conductivity of solid and liquid metals with good accuracy. The other two physical properties must be left open for the future owing to the time constraints of this Ph.D. project. Our goal, therefore, is to investigate solid and molten metals. The first series of measurements were carried out with three cylindrical bars made of copper, aluminum, and brass, whereas the second series of measurements were carried out with a special alloy named galinstan at room temperature and tin at 232°C in the lab.

To accomplish the aims and objectives of the project, the entire thesis has been structured as follows:

Chapter 2 presents the traditional methods that have been used up to now for measuring the electrical conductivity of solid and liquid metals.

Chapter 3 presents the fundamental theory for measuring the electrical conductivity of conductive materials and explains in detail the two experimental setups of Lorentz force sigmometry that were used for both solid and fluid measurements. Details of the Halbach magnet and the force measurement system are also explained in sections 3.4 and 3.5. Calibration of the force measurement system to find the calibration factor that transfer volt to newton has been done in 3.6. Following, the uncertainty of measurements has been explained in 3.7. The results from the solid measurements are presented in Chp. 4. The first setup was used to prove the ability of Lorentz force sigmometry to measure the electrical conductivity of solid metals, using copper and aluminum bars to calculate the calibration factor of the LOFOS setup. This calibration factor was then implemented into the equation to find the electrical conductivity of the brass bar.

In Chp. 5, the results from the fluid measurements are presented. The first series of measurements were done with the eutectic alloy galinstan $\text{Ga}^{67}\text{In}^{20.5}\text{Sn}^{12.5}$ at room temperature. It has the same function as the copper and aluminum bars in the solid measurements, which was to find the calibration factor because we changed the nozzle geometry of the filling funnel for fluid measurements. Then, we used this calibration factor to find the electrical conductivity of the molten tin.

Finally in chapter 6, we present some concluding remarks of the research and provide a brief overview and ideas for future work.

Chapter 2

State of the art

2.1 State of the art of electrical conductivity of solid metals

We present some of the most widely used methods of measuring conductivity in the branch of solid-state physics in this section [Lark-horovitz & Johnson, 1959]. Ohm's law: The potential difference across both the ends of a conductor will be directly proportional to the current flowing through that conductor [Consoliver & Mitchell, 1920], given that the physical conditions such as temperature and mechanical stress do not change. It is represented by the equation below.

$$V = I \cdot R \tag{2.1}$$

In the equation, R denotes the resistance, I denotes the electrical current, and the potential difference (voltage) across the ends of the conductor is denoted by V . Resistivity: The resistance, R , of a conductor is directly proportional to its length, L , and inversely proportional to its cross-sectional area, A , given that the temperature remains constant. It can be equated as follows:

$$R = \rho \frac{L}{A} \tag{2.2}$$

Here, ρ denotes the resistivity of the material of the conductor.

2.1.1 Two-probe method for measuring the electrical conductivity of solid metals

The resistivity of a solid can be calculated by measuring the range of voltage drop caused by the passage of a constant current provided by a current source, such as a DC battery, in a long parallel pipe-shaped sample having a uniform cross section. An AM meter is used to measure the current in the specimen, I . The potential difference, V , between the two ends of the specimen is measured using a voltmeter. If the length between the two ends of the specimen is denoted by L and A denotes the cross-sectional area, then the resistivity can be found by employing equations 2.1 and 2.2.

$$\rho = \frac{VA}{IL} \quad (2.3)$$

The conductivity of an object is denoted by σ , and it is defined as the inverse of the resistivity. Therefore, the conductivity can be calculated by using equation 2.3 as follows:

$$\sigma = \frac{IL}{VA} \quad (2.4)$$

where the current I is measured in amperes, the voltage drop V across the ends of the specimen is given in volts, and the length L of the sample is measured in meters.

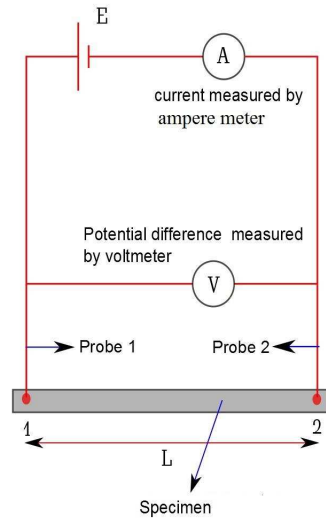


Figure 2.1: Two-probe method for measuring the electrical conductivity of a conductor. It consists of an AM meter to measure the current in the specimen and a voltmeter to measure the potential difference between the two ends of the long parallel pipe-shaped sample.

This method is not completely perfect, and it has some certain disadvantages. These disadvantages include the errors caused by the contact resistance between the measuring leads. Also, it is not possible to apply it to a simple shape and to certain types of samples. It is also quite difficult to solder the testing leads. Soldering creates impurities in the material while dealing with semiconductors, and therefore it also affects the intrinsic electrical resistivity.

A significant collinear equidistant four-probe method is used to overcome the two-probe method and its disadvantages. This method can measure the resistivity of conductors with different shapes but they should have a uniform cross section. To eliminate the errors discussed above, the soldering contacts are replaced by pressure contacts.

2.1.2 Four-probe method for measuring the electrical conductivity of solid metals

The four-probe method of measuring the electrical conductivity of solid metals comprises four equally spaced tungsten metal probes having a predetermined radius [Keithley, 2005]. All four probes are individually supported by springs on their ends so that the sampling damage during probing can be minimized. The sample is supplied with an electrical current through a high-impedance source

using the outer two tubes. A voltmeter is used to measure the voltage across the inner two probes. Given that the area of contact of every point is considered to be quite small, the contact area is not included in the calculations. For bulk sample with thickness much bigger than the probe spacing, we assume protrusion of current emanating from the outer probe tips. The conductivity is computed to be :

$$\sigma = \frac{I}{2\pi Va} \quad (2.5)$$

Here "a" denotes the distance between the probes.

Because of the high input impedance voltmeter, the inner probes do not draw any current from the circuit. Therefore, the voltage drop at points 2 and 3 are triggered by the contact resistance and are eliminated from potential measurements between the probes and the sample.

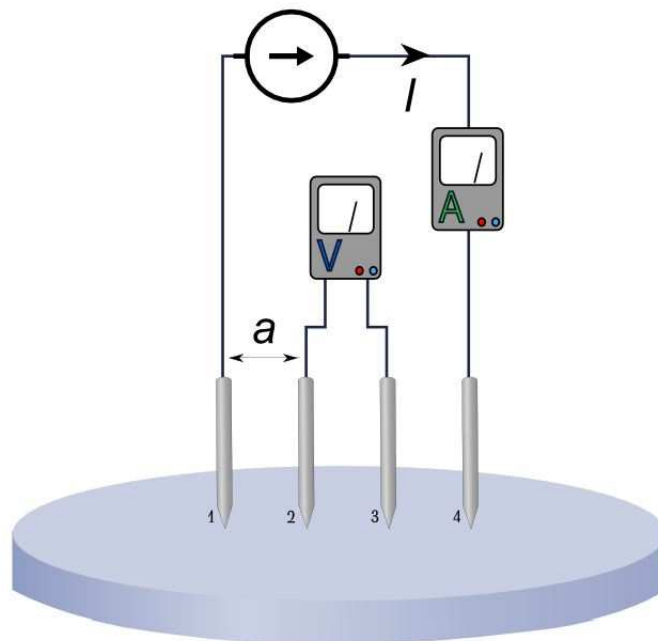


Figure 2.2: Four-probe method for measuring the electrical conductivity of a conductor. It consists of four equally spaced tungsten metal probes and two voltmeters (courtesy of Wikipedia).

In laboratory and industrial evaluations of semiconductors, the four-point probe technique is very widely used. Given that the apparatus is carefully and precisely constructed, the results obtained using this technique are possibly 5% more ac-

curate than two-probe method. This is not the best and recommended method where the chief considerations are reliability and reproducibility. There are many sources of error that can affect the accuracy of measurements [Keithley, 2005] such as electrostatic interference, leakage current, light and temperature. Some of these errors can be avoided, for example we can avoid the error due to light by placing the sample in dark chamber. The homogeneity of the sample, the probe geometry and size of the sample are also affecting the measurements accuracy. Using correction factors is very important for accurate measurements [Miccoli *et al.*, 2015]. Bowler & Huang [2005a] used this method to measure the electrical conductivity of metal plates and his measurements have an uncertainty of $\sim 0.5\%$. The four-point probe method has been determined to be very useful for studies of earth conductivity, in addition to its application on semiconductors.

2.1.3 Bridge methods [direct current (DC) and alternating current (AC)]

An additional method capable of determining the conductivity can precisely measure the resistance of the sample.

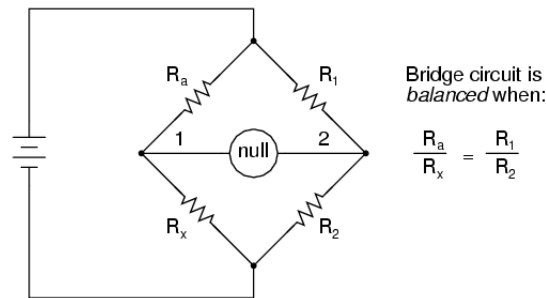


Figure 2.3: The Wheatstone bridge (direct current DC) consists of four resistances consists of four impedance.

An electrical circuit is used to measure the unknown electrical resistance by balancing the two legs of a Wheatstone bridge circuit in such a way that one of its legs includes the unknown component. The bridge will be balanced and the pointer will indicate zero when

$$R_a = R_x \frac{R_1}{R_2} \tag{2.6}$$

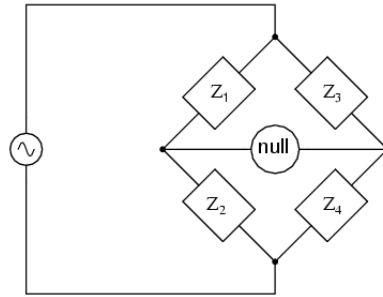


Figure 2.4: The Wheatstone bridge [alternating current (AC)].

DC measurements tend to show certain drawbacks, including polarization effects in ionic conductors and electrolytes, barriers at internal surfaces, and contact resistance, which arises in powders, films, and certain micellar structures such as selenium. Therefore, alternating current measurements are used to overcome the problems that arise in AC bridges. Impedances and resistances must be kept in proper balanced ratio. If we consider Z as a nonspecific impedance, then the AC bridge can be balanced if the impedance ratios of each branch are equal.

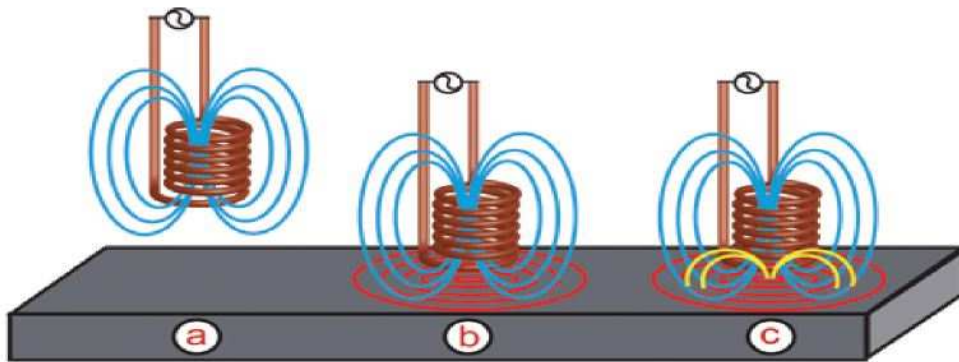
$$\frac{Z_1}{Z_2} = \frac{Z_3}{Z_4} \quad (2.7)$$

The impedance quantities in the abovementioned equation must be complex, accounting for both the magnitude and the phase angle. It is not enough that the impedance magnitudes alone are balanced. Without having the phase angles in balance as well, there will still be a voltage across the terminals of the null detector and the bridge will not be in a balanced state. The use of bridge techniques for conductivity measurements is much more restricted than the previously described probe methods.

2.1.4 Eddy current method

The eddy current testing method is based on the electromagnetic induction phenomenon of physics [Bean *et al.*, 1959; Bowler & Huang, 2005*b*]. In an eddy current probe, an alternating current is passed through a wire coil, which generates an oscillating magnetic field. If the probe and its magnetic field are brought close to a conductive material such as a metal test piece, a circular flow of electrons will then begin to move across the metal like swirling water in a stream, known as an eddy current. The eddy current that flows through the metal gen-

erates its own magnetic field, which then interacts with the coil and its field through mutual inductance. This reaction can be measured as a change in the impedance of the coil or sample arrangement. Figure 2.5 shows that the goal of eddy current testing is to determine the physical and metallurgical features (electrical conductivity, magnetic permeability, dimensions, coating, and defects) of the sample by the variation of impedance of the probe.



- a- magnetic field is generated (blue lines) by the alternating current which flows through the coil
- b- Eddy currents (red lines) are induced in the conductor when the coil is placed close to it
- c- The eddy currents in the material also produce their own magnetic field (Yellow lines) reacts to the coil, this reaction depends on the conductivity on materials surface and near-surface

Figure 2.5: Electrical conductivity measurement using the eddy current method (courtesy of Victor Aviation).

Eddy current sensing methodologies [Ma & Peyton, 2006]

I. Diffusion Phenomenon

The applied magnetic field will induce eddy currents inside the sample. This magnetic field will attenuate with depth δ which is mainly governed by the magnetic permeability μ , the electrical conductivity of the sample σ and the applied frequency f . For plane geometry sample, the attenuation is given by

$$\delta = \frac{1}{\sqrt{\pi f \mu \sigma}}. \quad (2.8)$$

For nonmagnetic electrically conductive sample, the magnetic permeability μ is

equal to $4\pi \times 10^{-7}$ H/m. Apparently, the low frequency measurements probes the surface of the sample deeper than the high frequency ones.

II. Coil impedance

The equation that describes the penetration of eddy currents into the sample is:

$$\nabla^2 A + j\omega\sigma A = -\mu J \quad (2.9)$$

where A is the magnetic vector potential, J denotes the current source density which passes through the excitation coil and ω is the angular frequency. So the physical principle of electromagnetic induction problems can be described as a diffusion equation in terms of A as given in a complex phasor notation for the sinusoidal waveform excitation cases by Eq. 2.9.

The electric field intensity E can be calculated through $E = \frac{\partial A}{\partial t}$. If we take the line integral of the vector E around the coil loop, we can calculate the induced voltage in sensing coil. An analytically solution to a circular coil of rectangular cross section above two-conductor plane has been done by Dodd & Deeds [1968]. The variation of real and imaginary impedance components of conductive sample under different values of reference number r/δ and lift-off (coil-to-sample spacing) is illustrated in Fig. 2.6. The reference number is defined as the ratio of mean coil radius r and skin depth δ .

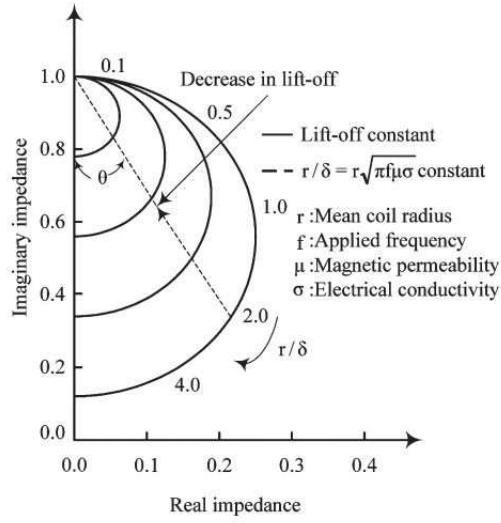


Figure 2.6: Normalized impedance curves for planar circular coil varying with reference numbers r/δ (coil radius/skin depth) and lift-off (coil-to-sample spacing)[Ma & Peyton, 2006].

Figure 2.6 shows that the reference number controls the data points shifting along the curve. The effect of decreasing lift-off causes the impedance curve to shrink, the smaller the value of lift-off, the closer the impedance curve approaches to the empty coil impedance point $(0, j)$. Apparently, the magnitude of eddy currents is dependent on the test geometry and as the phase angle θ is virtually lift-off invariant, so the phase signature is only dependent on the sample under test and indicates the existence of a relationship between phase angle θ and reference number r/δ .

III. Equivalent electrical conductivity

A linear relation has been observed between the cotangent of the phase angle and the reference number r/δ for a block sandwich-shaped sample under test using pancake coils.

$$\cot\theta = b + a\frac{r}{\delta} \quad (2.10)$$

Then, the electrical conductivity of the conductive sample can be measured by:

$$\sigma = \frac{(\cot\theta - b)^2}{\pi a^2 r^2 f} \quad (2.11)$$

where the parameters a and b in equations 2.10 and 2.11 depend on the coil sensor geometry and can be known from calibration using bulk materials with known electrical conductivity σ .

The eddy current method is presently being applied in commercial devices such as SigmaTest device. It is a very sensitive method when it comes to the variation of the distance between the sensor and the sample and the penetration depth of the magnet is limited by the skin effect.

Bowler & Huang [2005a] used this method to measure the electrical conductivity of brass and stainless steel plates. It is determined with 3 and 2 % uncertainty. This method has been used also in other applications like finding the defect in a conductive sample [Uhlig *et al.*, 2012b].

2.2 State of the art of electrical conductivity of fluid metals

Previous methods employed for measuring the electrical conductivity of molten metals can be divided into three groups:

- contact measurements
- containerless and contactless measurements
- contactless inductive measurements.

2.2.1 Contact measurements

In contact measurements, two- or four-probe sensors stay in direct contact with the sample. These probes are normally composed of platinum, molybdenum, etc., and they measure the potential drop of the constant current applied on the molten metal sample [Monaghan, 1999; Plevachuk *et al.*, 2006, 2008]. Some hot and aggressive molten metals may undergo dissolution and chemical reactions, after which there might not be a proper material for the probes to measure.

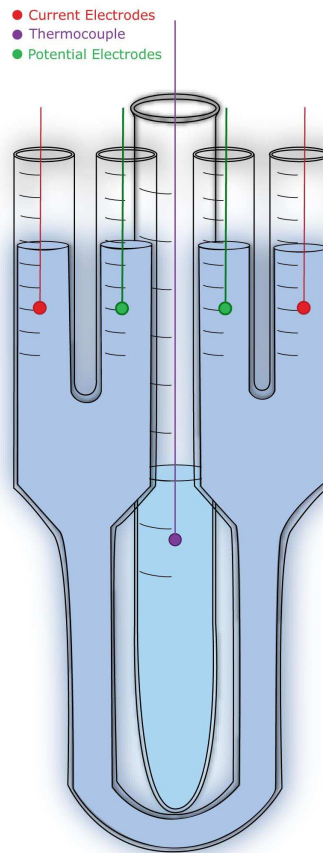


Figure 2.7: The four-probe method for electrical conductivity measurement of molten metal consists of two current electrodes, two potential electrodes, and one thermocouple.

[Monaghan, 1999] used this method to measure the electrical conductivity of gallium, tin, lead, copper, a lead tin alloy, a copper tin alloy, and a zinc alloy with uncertainty up to 1%. Updated and recent information about this method was presented at the MTLM-2015 conference in Dresden by Prof. Gasser, who claimed that he and his team can formulate a new probe material that can be used for any type of fluid that melts up to 1500 °C.

2.2.2 Containerless and Contactless Measurements

Electromagnetic levitation is used to measure the physical properties of a sample. In this method, the sample is levitated in air by a physical force (Lorentz force) against gravity (see Fig. 2.8). Thus, it is a containerless method. Then, the inductive method from the third group is used to measure the electrical con-

ductivity of the sample. The sample is placed in an alternating magnetic field inside a radiofrequency current carried on the primary coil. The induced voltage in the secondary coil depends on the electrical conductivity of the sample (see Fig. 2.9) . Marangoni convection [C.Marangoni, 1878] will occur if there is a temperature or concentration gradient on the surface. In addition, the levitation field also induces fluid flow in the sample. Therefore, the levitation method is only applicable to those cases where the absence of convection is not mandatory [Egry, 2004; Lohoefer, 2005; Richardsen *et al.*, 2002; Richardsen & Lohoefer, 1999].

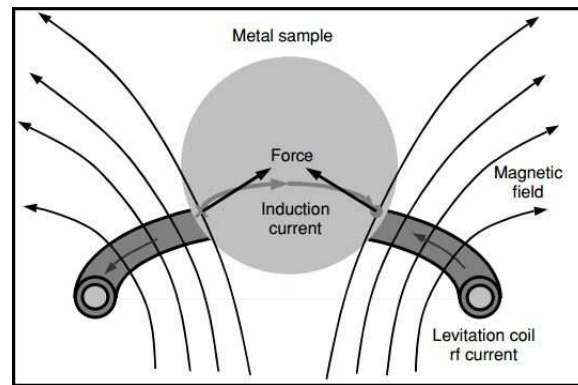


Figure 2.8: Principle of electromagnetic levitation. The rf magnetic levitation field induces eddy currents in the sample which, together with the field, generate Lorentz forces that support the sample against gravity [Lohoefer, 2005].

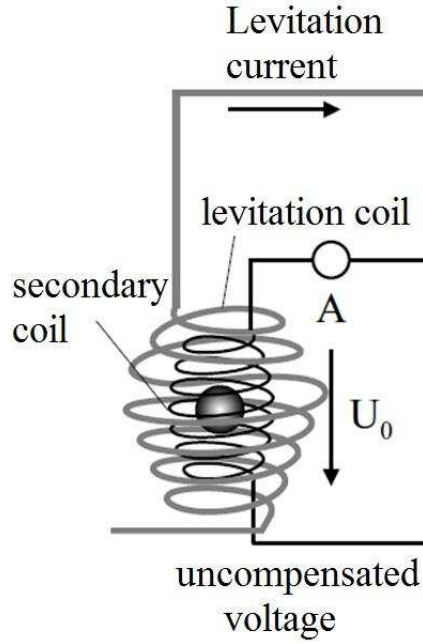


Figure 2.9: Schematics of electromagnetic levitation: the droplet is placed in an alternating magnetic field inside a radiofrequency current carried on the primary coil. The induced voltage in the secondary coil depends on the electrical conductivity of the sample.

Levitation is caused by the Lorentz force, F_L , given by [Seetharaman *et al.*, 2014]:

$$\vec{F}_L = \int (j_{ind} \times \vec{B}) dV \quad (2.12)$$

where j_{ind} is the current induced in the sample by the external electromagnetic field. The integral can be calculated in a multipole expansion [Edmonds, 1996; Thompson, 1994]. The relevant parameter for electromagnetic levitation is the skin depth δ , defined as :

$$\delta = \sqrt{\frac{2}{\omega \sigma \mu_0}} \quad (2.13)$$

here ω is the frequency of the alternating field, and μ_0 is the magnetic permeability constant.

A levitated liquid copper drop is shown in Fig 2.10. The levitation coil is inside a process chamber, and the levitated sample is illuminated by a laser beam in order to produce a shadow-graph of the sample for density measurements.

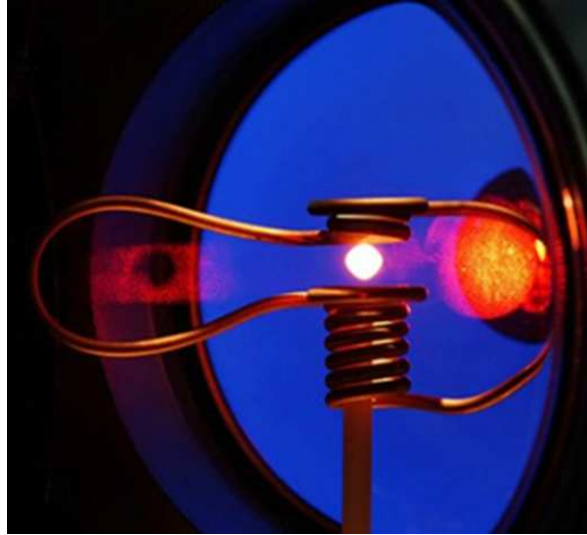


Figure 2.10: Picture of a hot electromagnetically levitated sample enclosed by the alternating current carrying levitation coil on the ground. The coil consists of a copper tube which is cooled from within by running water. The upper counterwinding prevents the lateral escape of the sample (courtesy of DLR-MP).

A clear study of uncertainty of measurements using this method has not been done by references.

2.2.3 Contactless inductive measurements

Braunbek [1932] was the first physicist to adopt the inductive method of measurement. This method is based on applying a rotating magnetic field to the sample, which induces the formation of circulating eddy currents. Consequently, the eddy currents will generate a damping torque directly proportional to the electrical conductivity [Bakhityarov & Overfelt, 1999; Chaberski, 1971; Delaney & Pippard, 1972]. Braunbek proposed the following relationship between the electric conductivity σ of the specimen and the mechanical moment caused by mutual interaction between the external magnetic field and an additional magnetic field induced by the eddy current:

$$M = \frac{\pi}{4}\sigma\omega LR^4 B^2 - \frac{\pi}{192\eta}\sigma^2\omega LR^6 B^4 \quad (2.14)$$

where M is the mechanical moment caused by mutual interaction between the external magnetic field and an additional magnetic field induced by the eddy current; L and R are the length and radius of the specimen, respectively; ω is the angular velocity of the rotating magnetic field; B is the magnetic induction; and η is the viscosity of the liquid specimen. According to Braunbek [1932], the magnetic induction and the dimensions of the specimen can be selected such that the second term in Eq. 2.15 becomes negligibly small as compared to the first term in the case of metals of unknown viscosity.

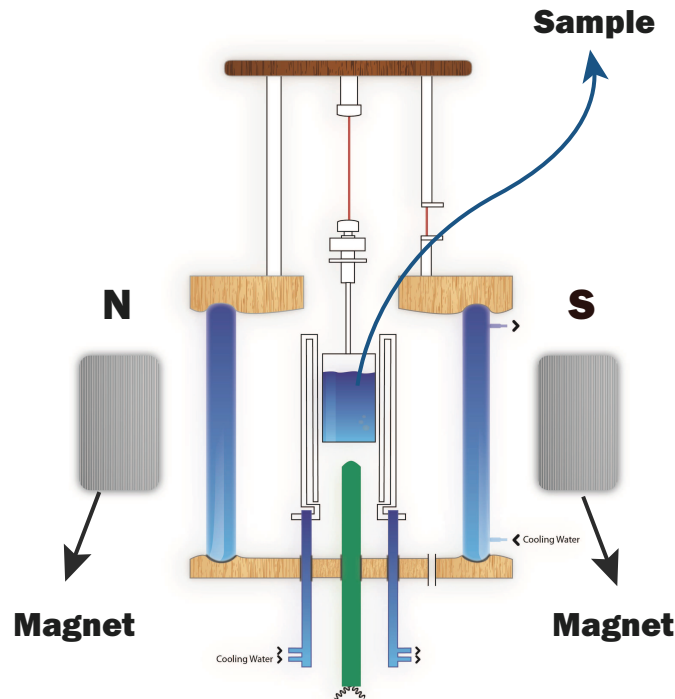


Figure 2.11: Inductive method using rotating magnetic field for measuring the electrical conductivity. It consists of a rotating magnetic field and a molten metal (sample) suspended by a rope and located inside the magnetic field. It measures the electrical conductivity of the sample by measuring the torque.

The uncertainty of measurements using rotating magnetic field is claim to be less than 0.5 % Braunbek [1932].

2. State of The Art

Chapter 3

Fundamentals and Experimental Setup

In this chapter, the fundamental equations used to calculate the electrical conductivity for both solid and molten metals is defined (section 3.1), followed by a presentation of the two experimental setups, one for molten metals (section 3.2) and the other for solid metals (section 3.3). The two setups consist of two main parts: the first part is to measure the Lorentz force signal using the Lorentz force apparatus (LOFOS-apparatus), and the second part consists of an electronic scale and the electronic devices (amplifiers, converters, voltmeters) and a computer for recording and analyzing the force and mass signal. More details about the different parts of the experimental setups, namely the Halbach magnet and the force measurement system, are described in sections 3.4 and 3.5. Calibration of the force measurement system is described in section 3.6 and uncertainties analysis is in section 3.7.

3.1 Fundamentals

The Lorentz force per unit volume is approximately $F \sim \sigma v B_0^2$, where σ is the electrical conductivity of the conductor, v is the velocity of the conductor, and B_0 is the magnitude of the magnetic field [Grant & Phillips, 1990]. To obtain the total Lorentz force, we multiply by the volume $r^2 L$, where r (radius of cross section) and L (height) are the dimensions of the area where the fluid flow interacts

3. Fundamentals and Experimental Setup

with the magnetic field:

$$F \sim \sigma v B_0^2 r^2 L \sim \sigma L B_0^2 Q \quad (3.1)$$

where Q is the volumetric flow rate, given as $Q = \pi r^2 v$

The mass flow rate is given by:

$$\dot{m} = \frac{Q}{\rho} \quad (3.2)$$

where ρ is the density of the conductor. Here, we introduce the calibration factor K :

$$K = \frac{1}{c L B_0^2} \quad (3.3)$$

where c is the dimensionless form coefficient accounting for the distribution of the magnetic field in LOFOS. By incorporating Eqs. 3.2 and 3.3 into Eq. 3.1, the basic equation linking the mass flow rate \dot{m} with the Lorentz force F generated by the magnetic field in the fluid can be obtained:

$$\dot{m}(t) = \frac{\rho K}{\sigma} F(t) \quad (3.4)$$

From Eq. 3.4, the cumulative mass during the operating time is determined as follows:

$$M = \int_{t_1}^{t_2} \dot{m}(t) dt = \frac{\rho K}{\sigma} \tilde{F} \quad (3.5)$$

where \tilde{F} is the integral of the Lorentz force over the process time. From Eq. 3.5, the final equation to calculate the electrical conductivity σ for molten metals can be derived:

$$\sigma = \rho K \frac{\tilde{F}}{M} \quad (3.6)$$

This equation can be also used for solid metals by considering that the cumulative mass M for solids can be immediately measured by weighing the bars with an accurate scale. The calibration factor K obtained from the preliminary test can be used for future experiments to measure the electrical conductivity of solid bars with the given design of the LOFOS apparatus.

3.2 Experimental setup for fluid measurements

The Lorentz force sismometry setup for measuring the electrical conductivity of fluid metals (see Figs. 3.1), and 3.2) comprises three main parts: (i) the filling funnel, where the molten metal is poured.

(ii) a collecting vessel placed over a scale connected to a computer for measuring the mass of the molten metal M , and (iii) an LOFOS-apparatus.

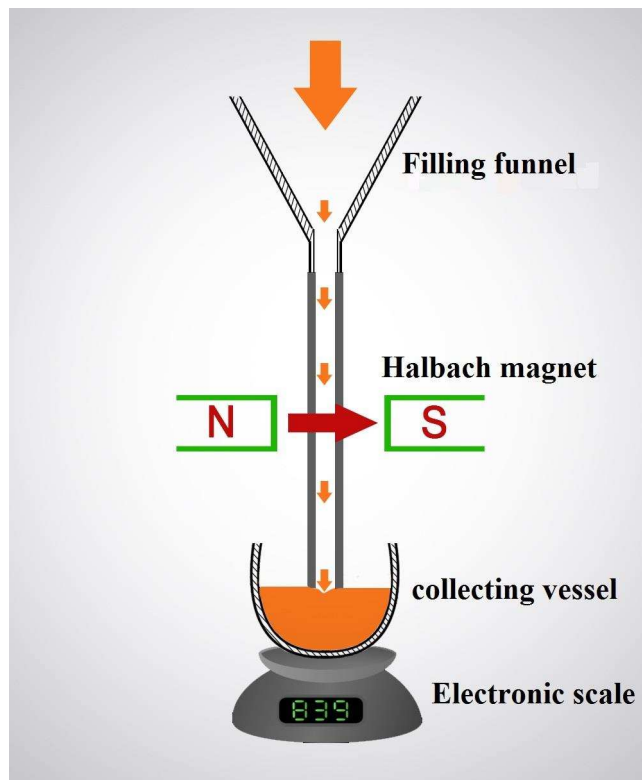


Figure 3.1: Two-dimensional (2D) schematic of the Lorentz force sismometry setup for measuring the electrical conductivity of molten metals. 1: filling funnel, 2: Halbach magnet, 3: collecting vessel, and 4: electronic scale.

3. Fundamentals and Experimental Setup

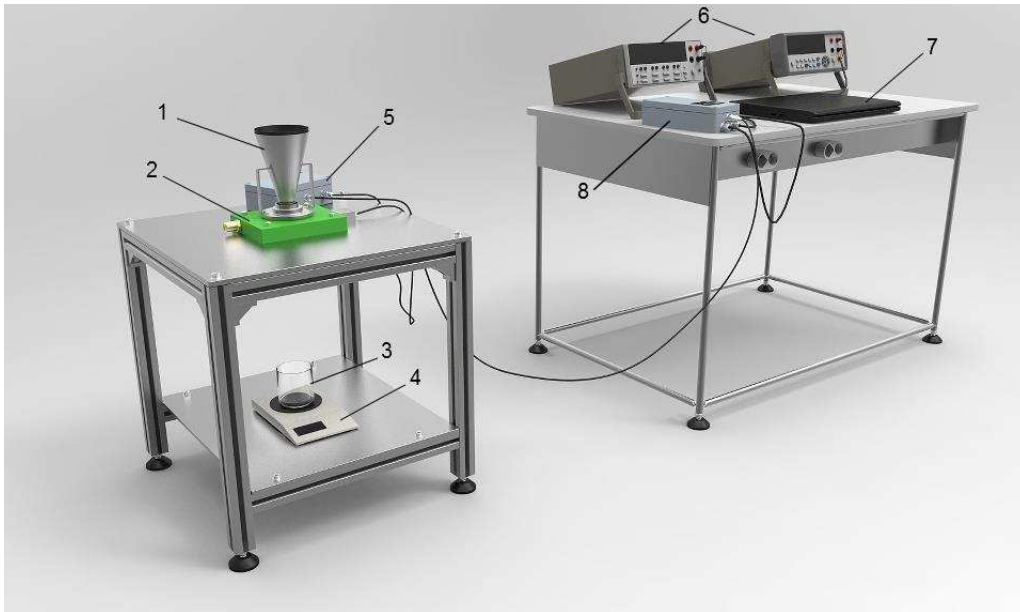


Figure 3.2: Three-dimensional (3D) schematic of the Lorentz force sismometry setup for measuring the electrical conductivity of molten metals. 1: filling funnel, 2: LOFOS-apparatus, 3: collecting vessel, 4: electronic scale, 5: amplifier and converter, 6: voltmeters, 7: computer, and 8: transformer and converter.

The LOFOS apparatus consists of several parts (Fig. 3.3):

Block-1 is a circular Halbach magnet, which is a special arrangement of small permanent magnets (12 small magnets in our case); this enhances the magnetic field on one side of the array (magnetic field induction $B_0 = 250$ mT), while cancelling the magnetic field on the other side. A TML strain gauge sensor is placed under the magnet to measure the force equal to the Lorentz force acting on it. Block-2 is a thermocouple sensor which is located near the magnet to measure the temperature in this area.

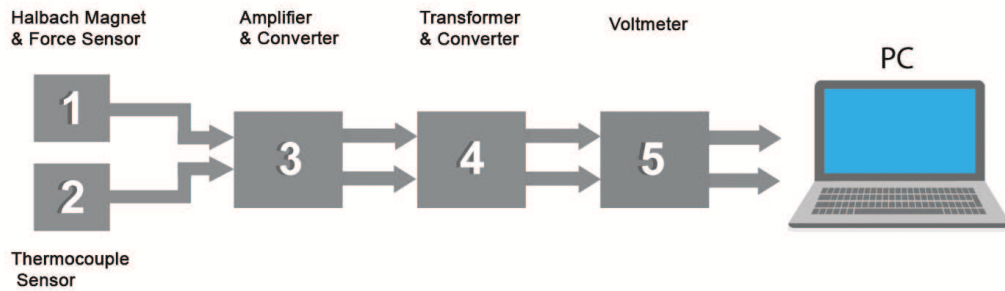


Figure 3.3: LOFOS-appartus diagram; 1: Circular Halbach magnet and force sensor, 2: thermocouple sensor, 3: amplifier and converter, 4: converter and transformer, 5: voltmeter, 6: computer.

Block-3 is an electronic box that performs many functions, such as supplying power to the force sensor. It has two amplifying channels that amplify the signals of both sensors. Block-4 has two indicators that display the temperature and Lorentz force value. It transforms the digital signal into an analog signal. Block-5 is a Keithley voltmeter model 2700 with a wide voltage measurement range [from 100 nV to 750 V], which reads the force signal and sends it to the computer; here, a special LabVIEW code reads and displays the analog signal of the Lorentz force.

3.3 Experimental setup for solid measurements

We used the same Lorentz force sgmometry setup for measuring the electrical conductivity of fluid metals for solids but with some technical changes (see Figs. 3.4 and 3.5)

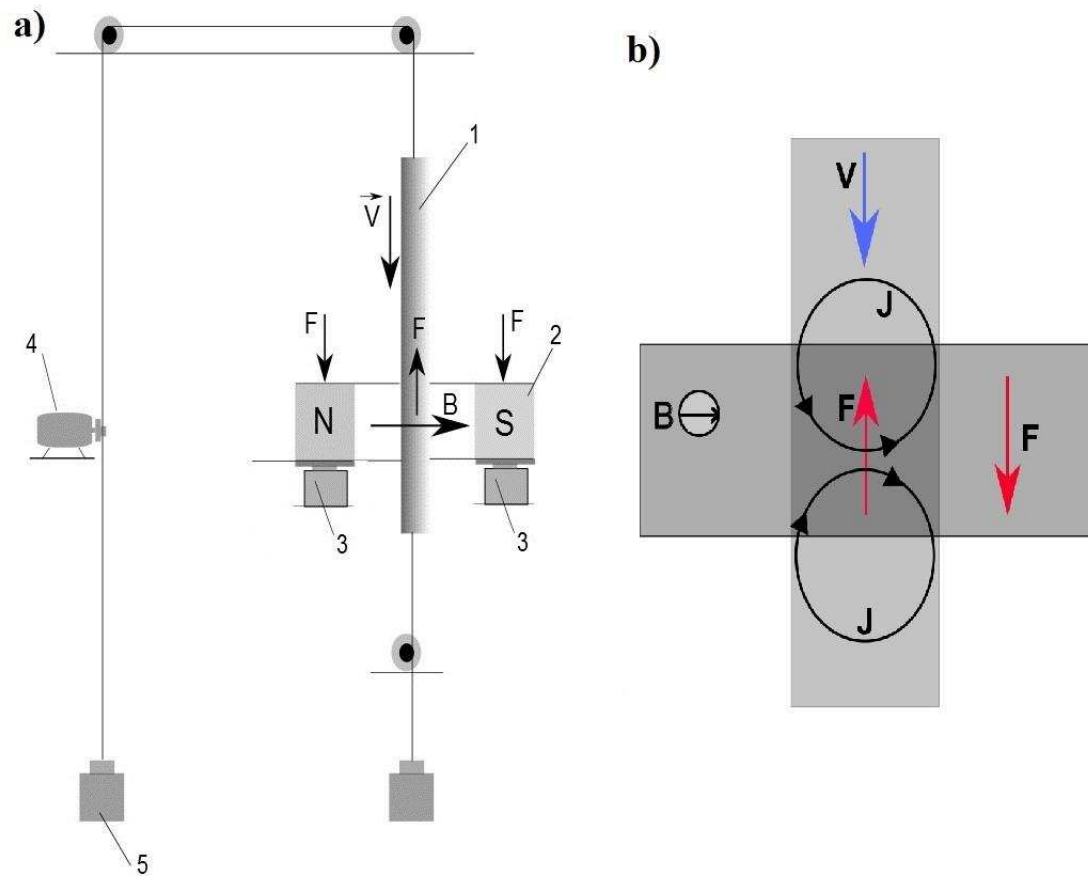


Figure 3.4: (a) Two-dimensional (2D) schematic of Lorentz Force Sigmometry setup for electrical conductivity measurements of solid metals. 1: sample of a solid metal, 2: Halbach magnet, 3: force sensor, 4: Mädler motor, 5: weight. (b) A braking force acts on the conducting bar and is matched by an accelerating force on the magnet.

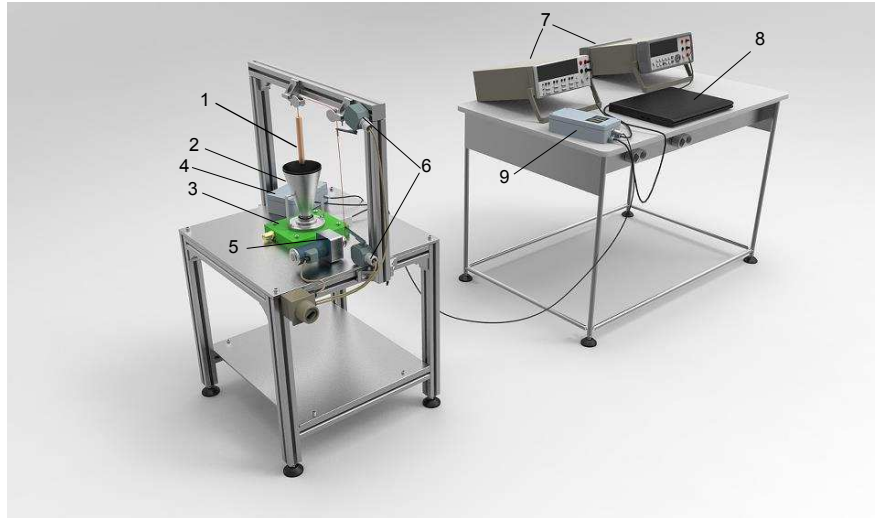


Figure 3.5: Solid metals setup: three-dimensional (3D) schematic of Lorentz force sismometry setup for measuring the electrical conductivity of solid metals; it consists of 1- sample of a solid material, 2- filling funnel, 3- LOFOS-apparatus, 4- amplifier and converter, 5- Mädler motor, 6- stop elements, 7- voltmeters, 8- computer, 9- transformer and converter.

A Mädler small-g geared motor type GE/I with an AC capacitor was connected to the solid bar by a rope passing through two plastic rollers. We used two stop elements to stop the rotation of the motor in both directions automatically. The rotation speed of the motor was controlled by a voltage controller, by increasing or decreasing the voltage input, or by changing the motor cylinder size (a smaller size corresponds a slower rotation, and vice versa). The linear speed of the bar was 10 cm s^{-1} . The mass M of the bars is measured separately using an accurate scale before the experiment; we hung two weights at both ends of the rope to have an equal weight in both directions. If the weight on the side of the motor is W_1 , the weight of the bar is W_2 ; then, a weight $W_3 = W_1 - W_2$ would be necessary necessary on the side of the bar to achieve perfect balance. Two voltmeters were connected to the LOFOS apparatus to read the measurements from both sensors, i.e., the force signal and the temperature near the force sensor.

3.4 Halbach cylinder magnet

A Halbach array is a special configuration of small permanent magnets that maximizes the magnetic field on one side while cancelling it to zero on the other side. It was invented by Klaus Halbach in the 1980s at the Lawrence Berkeley National Laboratory for a specific application: focusing particle beams without using coils.

3. Fundamentals and Experimental Setup

Since then it has been widely used in generators, motors, magnetic bearings, and many more applications.

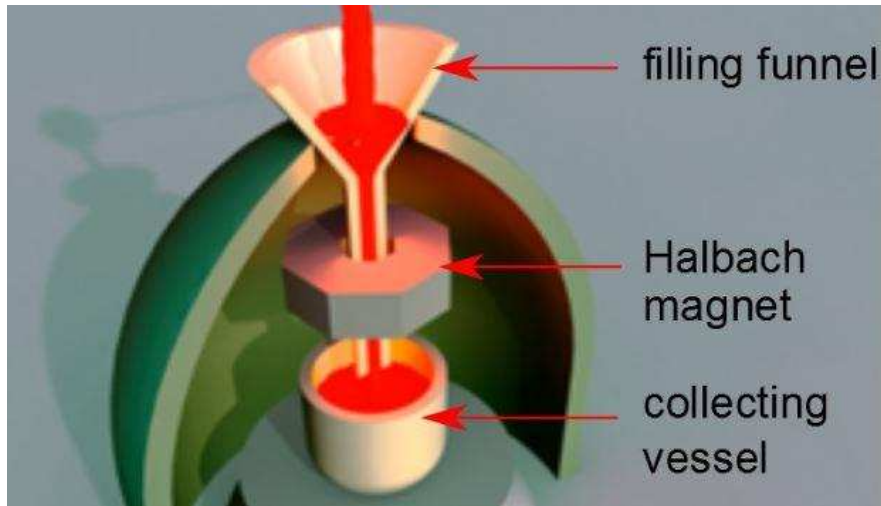


Figure 3.6: A zoom in of 3D schematic of Lorentz force siphonometry showing the Halbach cylinder surrounding the nozzle of the filling funnel.

A Halbach array has many forms, different numbers of magnets, N , different sizes, and different magnetic field flux densities. One needs to find the optimal Halbach configuration for the application of interest. Weidemann [2013] in his Ph.D. dissertation carried out both an analytical and a simulation study for different types of cylindrical Halbach arrays (8, 12, and 16 trapezoidal segments). In Fig. 3.7, we see the magnetic field induction magnitude in a cylindrical Halbach array with 8 trapezoidal segments.

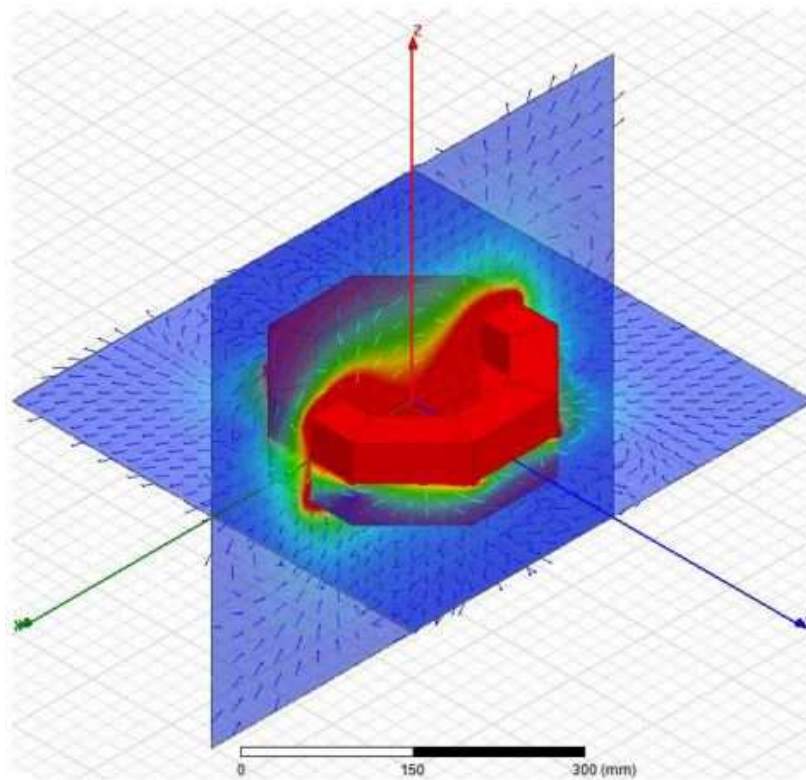


Figure 3.7: FEM model of cylindrical Halbach array with 8 magnets. The colored domains indicate the magnitude of the magnetic induction. [Weidermann, 2013].

Another important factor in choosing the optimum Halbach cylinder is the non-dimensional shape factor, γ , which is the ratio of the outer radius, R_0 , to the inner radius, R_i , of the polygonal cross section of the Halbach cylinder (see Fig. 3.8a). Weidermann calculated the Lorentz force generated by different Halbach cylinder designs, and he found that the Lorentz force was greater for higher numbers of small magnets, N . The maximum force was obtained when γ equaled 1.5, as shown in Fig. 3.8b.

3. Fundamentals and Experimental Setup

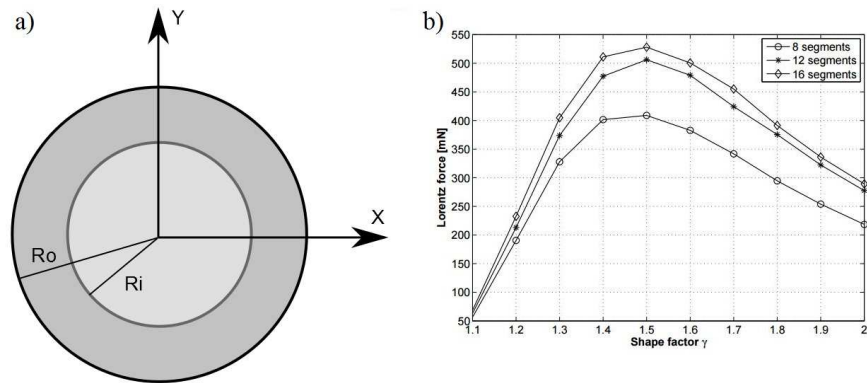


Figure 3.8: (a) Cross section of cylindrical Halbach magnet in x - y plane shows the radii, R_i and R_o for the inner and outer circles, respectively. (b) Optimization of Lorentz force generation using Halbach cylinder magnet system. Three magnetization patterns with 8, 12, and 16 trapezoidal segments [Weidermann, 2013].

However, for the Lorentz force sigmometry setup, we chose the cylindrical ring form, in which the magnetic field was trapped inside the ring (see Fig. 3.9, red box) with 12 permanent magnets and a magnetic field flux density equals to 250 mT.

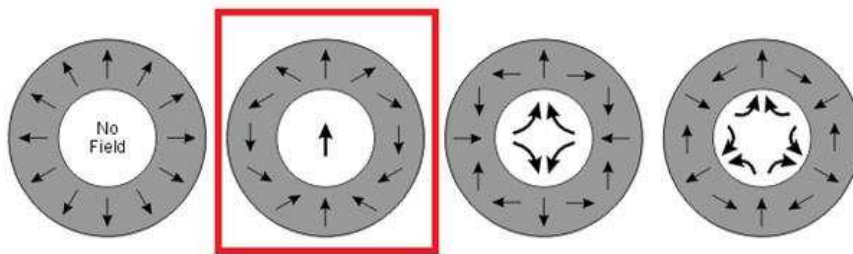


Figure 3.9: Ferromagnetic cylinder showing various magnetization patterns and magnetic fields. The red box refers to the type used in the current Lorentz force sigmometry setup. (courtesy of Wikipedia).

Figure 3.9 shows that for a 12-element cylindrical Halbach, we have four options for the magnetic field distribution just by changing the orientation of the magnetization of the small permanent magnets. The magnetic induction distribution for the chosen Halbach cylinder shows moderate gradients along the x -axis, and it is reasonably constant along the y -axis (see Fig. 3.10).

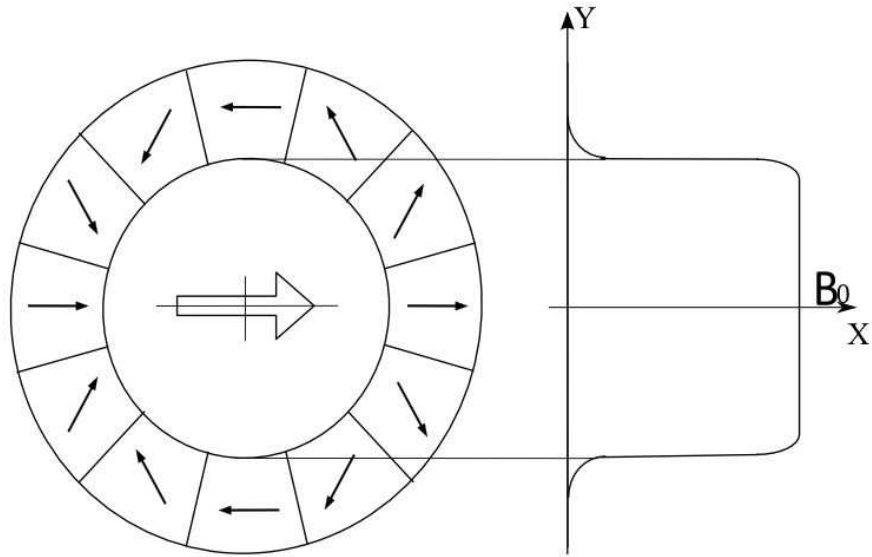


Figure 3.10: Magnetic field distribution in the inner space of the Halbach magnet. The arrows show the magnetization direction of the magnet elements.

Here, we present the exact dimensions of the Halbach cylinder with its parts that has been used in Lorentz force sigmometry setup (Fig. 3.11). We also study the effect of the iron housing on the magnetic field distribution, as shown in Fig. 3.11.

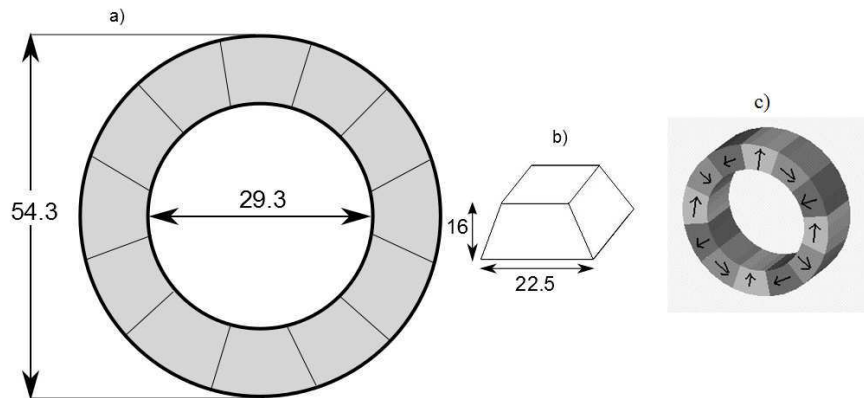


Figure 3.11: Design of the magnet system. a) The top view shows the diameters of the inner and outer circles and b) the single magnet segment. c) Three-dimensional schematic of the Halbach cylinder.

3. Fundamentals and Experimental Setup

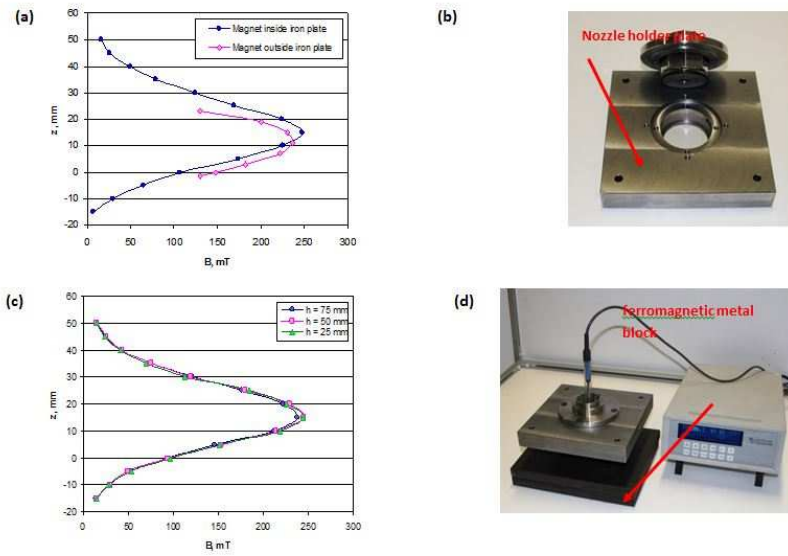


Figure 3.12: Influence of ferromagnetic materials on the magnetic field distribution. (a) Dependence of the transversal component of the magnetic field from the axial coordinate along the symmetry axis of the magnet system itself, as well as for the magnet system if installed in the nozzle holder plate, which is shown in (b). (c) Dependence of the transversal component of the magnetic field from the axial coordinate along the symmetry axis for the magnet system installed in the nozzle holder plate under the additional influence of the ferromagnetic iron block at a distance h from the bottom edge of the nozzle holder plate [shown in (d)].



Figure 3.13: Photo of Halbach cylinder magnet system picture. It shows its different; parts housing lower part, housing top and the twelve symmetrically aligned trapezoidal permanent magnets.

Figure 3.13 shows the upper and lower parts of the housing of Halbach magnet. In the lower part located supporting sharp needles which enable a frictionless turn of the magnet.

3.5 Force measurement system

A strain gauge is the sensor that has been used in the measurement system for Lorentz force sismometry. It consists of a metallic foil which surrounded by an isolating backing. Its work principle can be explained as follows (see Fig. 3.14). If a strip of conductive metal is stretched, it will become skinnier and longer, both changes resulting in an increase of electrical resistance end-to-end. Conversely, if a strip of conductive metal is placed under compressive force (without buckling), it will broaden and shorten. If these stresses are kept within the elastic limit of the metal strip (so that the strip does not permanently deform), the strip can be used as a measuring element for physical force, the amount of applied force inferred from measuring its resistance.

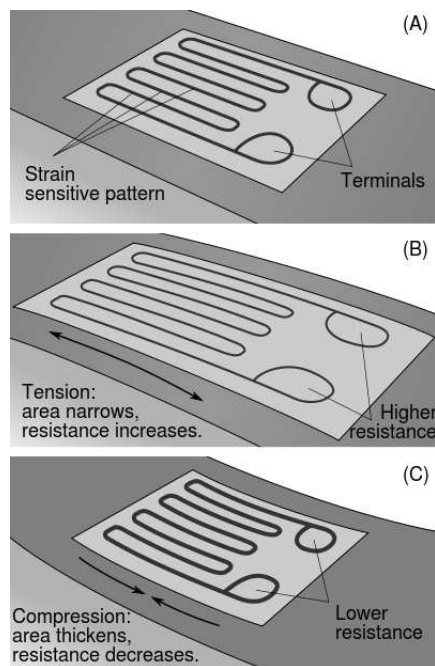


Figure 3.14: A sketch explaining the working principle of the strain gauge under exaggerated bending (courtesy of Wikipedia).

Typical strain gauge resistances range from $30\ \Omega$ to $3\ \text{k}\Omega$ (unstressed). This resistance may change only a fraction of a percent for the full force range of the gauge, given the limitations imposed by the elastic limits of the gauge material and of the test specimen. Forces great enough to induce greater resistance would permanently deform the test specimen and/or the gauge conductor itself, so ruining the gauge as a measurement device. Thus, in order to use the strain gauge as a practical instrument, we must measure extremely small changes in resistance

3. Fundamentals and Experimental Setup

with high accuracy. Such demanding precision calls for a bridge measurement circuit.

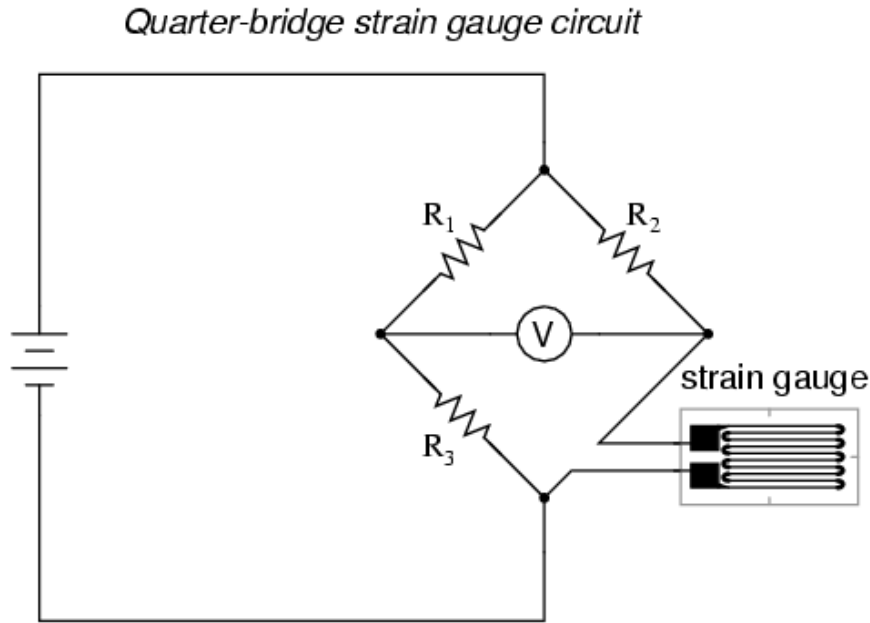


Figure 3.15: Bridge strain gauge circuit (courtesy of Allaboutcircuit website).

Typically, the resistance R_2 of the bridge is set at a value equal to the strain gauge resistance with no force applied, and (R_1 and R_3) are set equal to each other. Thus, with no force applied to the strain gauge, the bridge will be symmetrically balanced and the voltmeter will indicate zero volts, representing zero force on the strain gauge. As the strain gauge is either compressed or tensed, its resistance will decrease or increase, respectively, thus unbalancing the bridge and producing an indication at the voltmeter. As we used cylindrical Halbach magnet, we found that it was necessary to use three bridge strain gauge circuits in three positions, but they work as one bridge (see Fig. 3.16).

3. Fundamentals and Experimental Setup

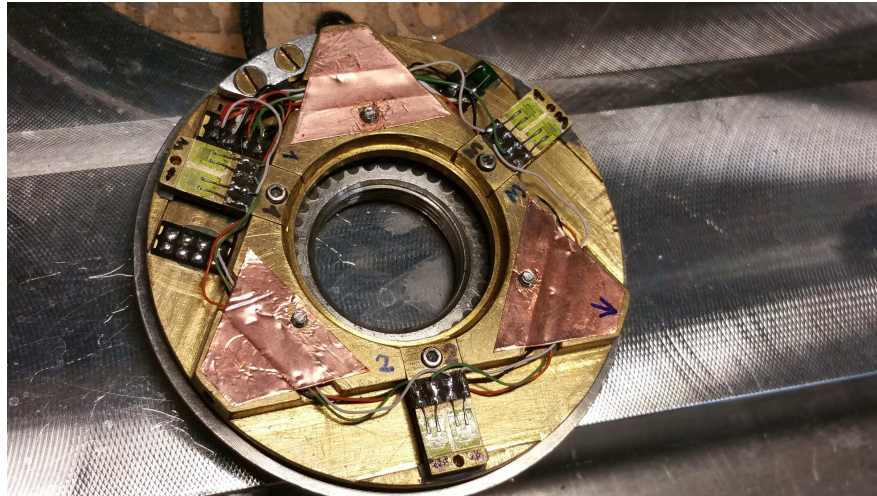


Figure 3.16: Photograph of the force measurement system of the Lorentz force sismometry, which consisted of three bridge strain gauge circuits working as one sensor to measure the Lorentz force of the moving conductive material.

The Halbach magnet, which was explained in the previous section, was installed above the sensor measurement system, as shown in next photo:

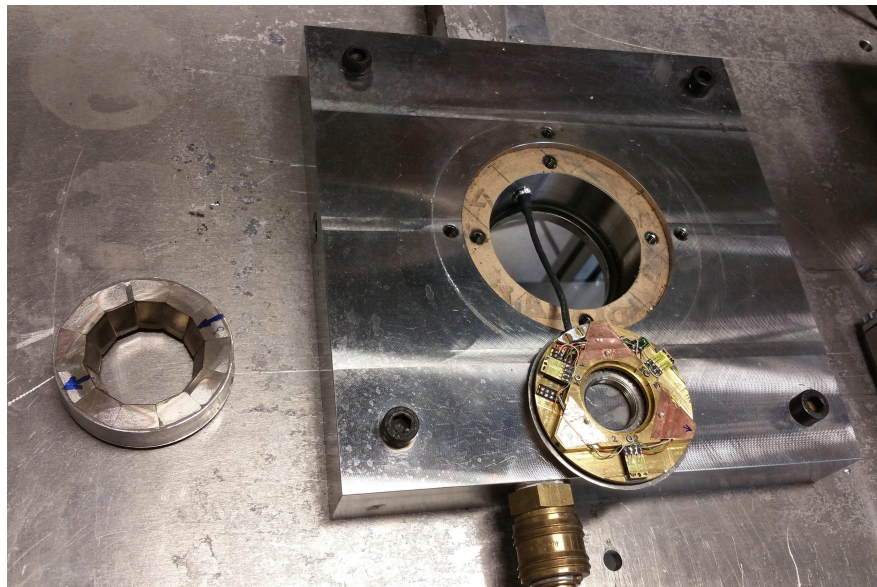


Figure 3.17: Photograph of force measurement system of Lorentz force sismometry during installation.

After designing the magnet system and the sensor system, calibration was needed in order to calculate the error of the force measurement.

3.6 Calibration of Lorentz force sigmometry device

The goal of calibration process to LOFOS force measurement is to find the calibration factor that convert voltage to newton. We put different weight over the magnet system located over the force measurements and record the corresponding force (see Fig. 3.18). Knowing that the gravity acceleration on earth is different for different places due to the height from sea level, we need to know the exact gravity in Ilmenau city, which is located 478 m above the sea level. For this, we used the data base from gravity information system PTB [Physikalisch-Technische Bundesanstalt, 2006].

The gravity acceleration in Ilmenau is 9.8101 m s^{-2} with uncertainty of ± 0.00002 .

If we use Newton's second law for the gravity force $F = m \cdot a$, where F is the force applied in newton, m is the mass of the object receiving the force in kilogram, and a is the acceleration of the object, then:

$$1 \text{ N} = 1 \text{ kg} \cdot \text{m s}^{-2}$$

At average gravity on earth, ($g = 9.8101 \text{ m s}^{-2}$ for Ilmenau), a kilogram mass exerts a force of about 9.8101 newtons. Now, we know the formula to convert the grams to Newtons, we can start the calibration using 0.5 g, 1 g, 5 g, 10 g, 20 g and 50 g weight over the measurement system, record the force in voltage and then calculate the calibration factor.

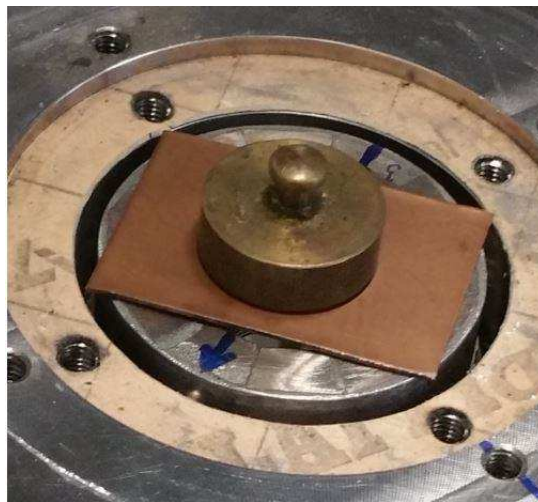


Figure 3.18: Photo of force measurement system calibration of Lorentz force sigmometry. This photo shows a weight equals to 50 g over the measurement system.

3. Fundamentals and Experimental Setup

Table 3.1: LOFOS force sensor measurements in volt when different weights placed over the force sensor in comparison to reference values in newton

Weight [g]	LOFOS sensor measurements [V]	Reference value [N]
0.50031 ± 0.00001	0.000478	0.004908
1.00121 ± 0.00004	0.000957	0.009822
5.00252 ± 0.00003	0.004814	0.049075
10.0069 ± 0.00002	0.009614	0.098168
20.01513 ± 0.00009	0.019164	0.196350
50.01158 ± 0.00013	0.047794	0.490618

Now, we can calculate the calibration factor by calculating the slope of the Newton–Volt measurement results (see Fig. 3.19).

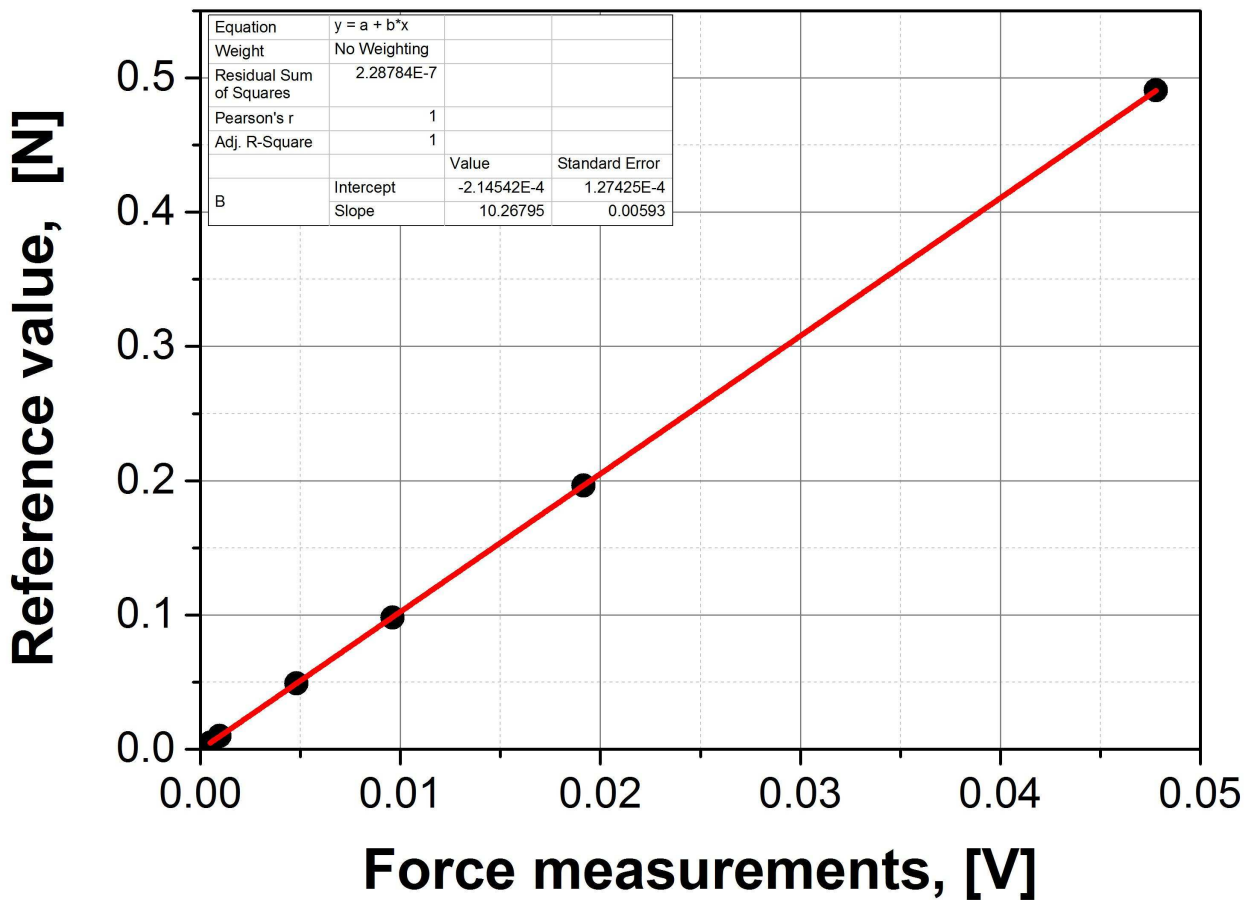


Figure 3.19: Linear fit of force sensor measurements in volt using LOFOS with the reference values in newton in order to calculate the slope which equals to the calibration factor.

As we see from Fig. 3.19, the calibration factor is 10.26795 ± 0.0059 [N V⁻¹].

3.7 Uncertainties analysis

The random error of measurements can be estimated by the standard deviation of the mean [Taylor, 1997].

If the measured value is X and the mean value of the N number of measurements is \bar{X} , then the standard deviation of the mean value is:

$$\delta(\bar{X}) = \frac{\delta(X)}{\sqrt{N}} \quad (3.7)$$

where the mean can be calculated as follows:

$$\bar{X} = \frac{1}{N} \sum_{i=1}^N X_i \quad (3.8)$$

The random error often has a Gaussian normal distribution, where 68% of the measurements lie in the interval $\bar{X} - \delta(\bar{X}) < X < \bar{X} + \delta(\bar{X})$

The standard deviation of the measured value X is:

$$\delta(X) = \sqrt{\frac{1}{N-1} \sum_{i=1}^N (X_i - \bar{X})^2} \quad (3.9)$$

so the measured value X can be represented as:

$$X = \bar{X} \pm \delta(\bar{X}) \quad (3.10)$$

If Y is a function of i variables x_n and these variables are independently affecting

3. Fundamentals and Experimental Setup

the function with random error, then the total error

$$\delta(Y) = \sqrt{\sum_{n=1}^i \left(\frac{\partial Y}{\partial x_n} \delta(x_n)\right)^2} \quad (3.11)$$

Fortunately for our measurements in chapter 4 and 5, the error of measurements coming from independent variable so that we can use the Eq. 3.11 to calculate its uncertainty.

Here, we shows one example of this error analysis and we will follow the same steps for other measurements in chapter 4 and 5 and added it directly.

We calculate the calibration factor K (see Eq. 3.12) for copper bar:

$$K = \frac{\sigma M}{\rho \tilde{F}} \quad (3.12)$$

Using Eq. 3.11 to calculate $\delta(\overline{K})$:

$$\delta(\overline{K}) = \sqrt{\left(\frac{\partial \overline{K}}{\partial \overline{\sigma}} \delta(\overline{\sigma})\right)^2 + \left(\frac{\partial \overline{K}}{\partial \overline{M}} \delta(\overline{M})\right)^2 + \left(\frac{\partial \overline{K}}{\partial \overline{\rho}} \delta(\overline{\rho})\right)^2 + \left(\frac{\partial \overline{K}}{\partial \overline{\tilde{F}}} \delta(\overline{\tilde{F}})\right)^2} \quad (3.13)$$

$$\delta(\overline{K}) = \sqrt{\left(\frac{\overline{M}}{\rho \cdot \tilde{F}} \delta(\overline{\sigma})\right)^2 + \left(\frac{\overline{\sigma}}{\rho \cdot \tilde{F}} \delta(\overline{M})\right)^2 + \left(-\frac{\overline{\sigma} \cdot \overline{M}}{\tilde{F} \cdot (\overline{\rho})^2} \delta(\overline{\rho})\right)^2 + \left(-\frac{\overline{\sigma} \cdot \overline{M}}{\overline{\rho} \cdot (\tilde{F})^2} \delta(\overline{\tilde{F}})\right)^2} \quad (3.14)$$

Now if we divide the both side of Eq. 3.14 by the mean calibration factor \overline{K} , we get what's called the relative measurement uncertainty of the calibration factor K :

$$\eta(K) = \frac{\delta(\overline{K})}{\overline{K}} = \sqrt{\left(\frac{\delta(\overline{\sigma})}{\overline{\sigma}}\right)^2 + \left(\frac{\delta(\overline{M})}{\overline{M}}\right)^2 + \left(\frac{\delta(\overline{\rho})}{\overline{\rho}}\right)^2 + \left(\frac{\delta(\overline{\tilde{F}})}{\overline{\tilde{F}}}\right)^2} \quad (3.15)$$

The source of the relative uncertainty of the electrical conductivity σ is mainly a reason of the random error (standard deviation) of ten measurements using SigmaTest device.

3. Fundamentals and Experimental Setup

The source of error for mass measurements is the random error of measuring the mass of copper bar ten times using electronic scale while the source error for density measurements is the error of the mass and volume of the copper bar. The source of the relative uncertainty of the integral of Lorentz force \tilde{F} is from the random error of all force measurements plus the uncertainty of the calibration factor that convert volt to newton. This converter factor has uncertainty due to mass uncertainty measurements and gravity uncertainty and the standard deviation error (see section 3.6).

We can rewrite Eq. 3.15 as follows:

$$\eta(K) \leq \eta(\sigma) + \eta(M) + \eta(\rho) + \eta(\tilde{F}) \quad (3.16)$$

So the relative uncertainty of calibration factor is less than 3.8 %:

$$\eta(K) = \frac{\delta(\bar{K})}{\bar{K}} \leq 0.49\% + 0.014\% + 0.6\% + 2.6\% \leq 3.8\% \quad (3.17)$$

We repeat these steps for calculating the relative uncertainty for all measurements that have been done and add them directly in Chp. 4 and Chp. 5.

Chapter 4

Electrical conductivity measurements of solid metals

This chapter presents the results obtained with the Lorentz force sigmometry for solid metals setup. We initially tested the device with short cylindrical bars made of copper, aluminum, and brass using the free-fall method. The test procedure and the initial results are presented in detail in section 4.1. We then made some technical changes to the device in order to improve the results and repeated the measurements with longer bars. The measurement procedure with the new device is explained in detail in section 4.2. We conducted two series of measurements. The first measurements were used to determine the calibration factor of the given LOFOS geometry with copper and aluminum cylindrical bars. These results are presented in section 4.3. The second measurements, given in section 4.4, were conducted with a brass bar to determine its electrical conductivity using the calibration factor obtained in the first experiment. The results of this section (solid measurements) have been published [Alkhalil *et al.*, 2015].

4.1 First test of the device / short solid bars measurements

For this test, we prepared three cylindrical bars made of copper, aluminum and brass with the same geometry (length = 149.7 ± 0.4 mm, diameter = 9.98 ± 0.03 mm).

4. Electrical Conductivity Measurements of Solid Metals

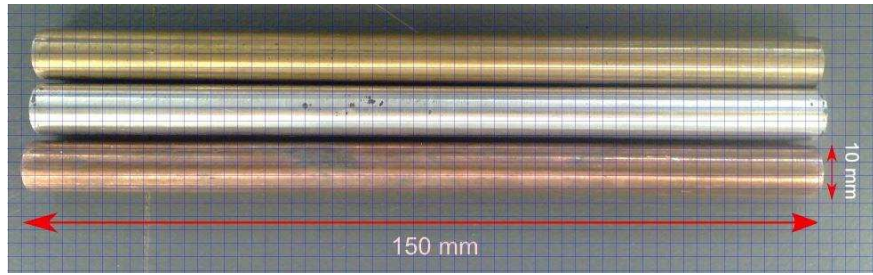


Figure 4.1: Three cylindrical bars made of copper(red), aluminum(gray) and brass(yellow). They have identical dimensions: $L = 150$ mm and $Q = 10$ mm. (taken with a camera).

The solid bar was fixed, but at time $t = 0$ s, it was disconnected and accelerated by gravity, $g = 9.8101 \text{ m s}^{-2}$ into the filling funnel with a 12 mm diameter nozzle, passing the magnetic field with a free-fall velocity of 0.2 m s^{-1} (see Fig. 4.2). Thus, the time of interaction between the bar and the magnetic field was very short, less than 1 s (750 ms). We recorded the Lorentz force signal simultaneously.

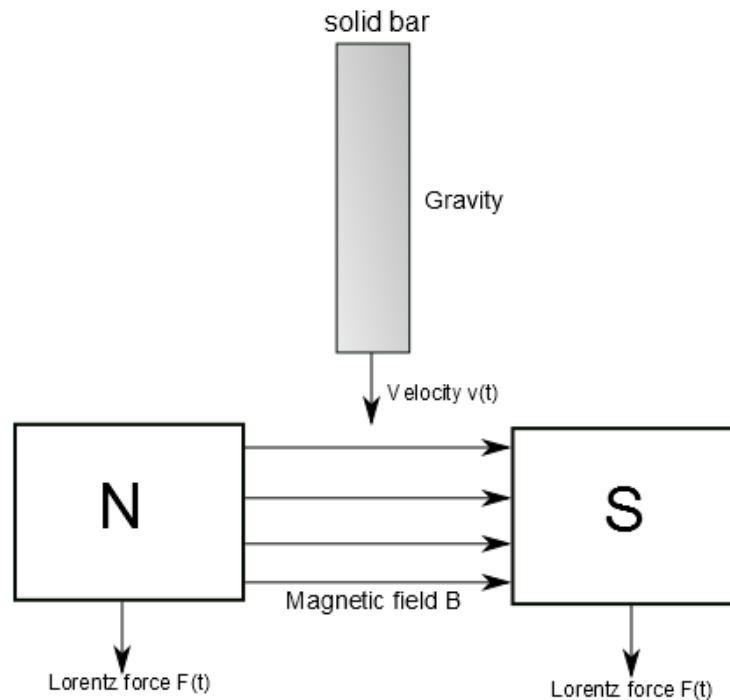


Figure 4.2: Illustration of the first test experiment. The solid bar is accelerated by gravity and passes the magnetic field lines with a velocity of 0.2 m s^{-1} . The Lorentz force acts to slow the conductor movement, while simultaneously another force equal to the Lorentz force acts on the magnet.

Even for this short time, we could register the Lorentz force for the bars (see Fig. 4.3). The figure shows that when the bar was outside the magnetic field, the Lorentz force was equal to zero; then, when the bar passed through the magnetic field, the force increased and remained stable for a very short period time as the bar passed through the magnetic area very fast. When the whole bar had passed through the magnetic field, the force returned to zero. However, the sampling rate is rather small (5 Hz). In future measurements, we plan to increase the sampling rate in order to collect more information from the signal.

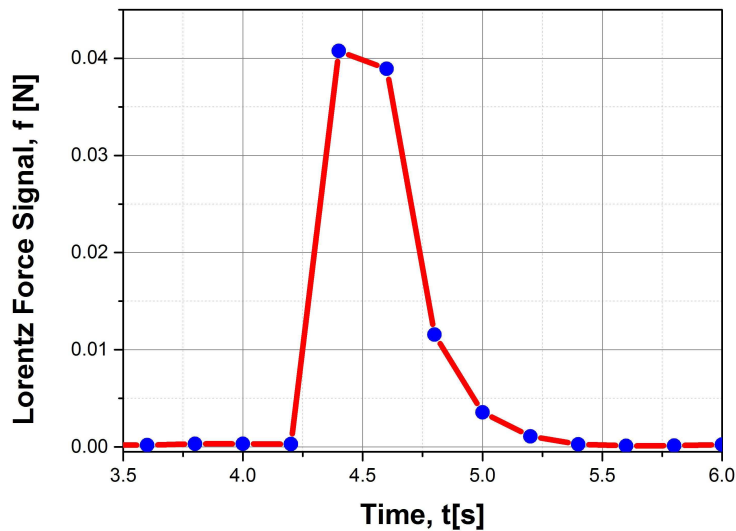


Figure 4.3: Lorentz force signal for copper bar when it passes the magnetic field with gravity acceleration (free-fall velocity).

In some cases, we obtained a single peak signal (Fig. 4.4). This is because the bar did not pass the magnetic field with the proper orientation (vertical, without touching the walls) and the sensor was unable to record the Lorentz force. The time that the Lorentz force amplitude is constant for all bars was very short and insufficient for accurate results, so we needed to decrease the velocity of the bar in order to increase the interaction time between the conductor and the magnetic field. In order to achieve better results, we made some technical changes to the setup (see Fig. 4.5) and repeated the experiments.

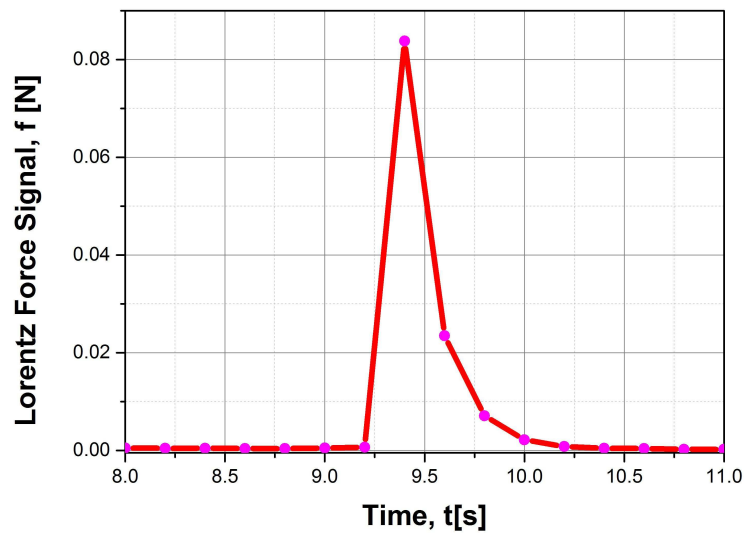


Figure 4.4: Lorentz force signal for copper bar when it passes the magnetic field with gravity acceleration (free-fall velocity). It is a single peak signal because the orientation of the bar as it passed through the magnetic field was incorrect.

4.2 Measurement procedure with long solid bars

The setup for this experiment has been explained in detail in a previous chapter (section 3.3). We repeat the figure in this section so the reader can follow the procedure better.

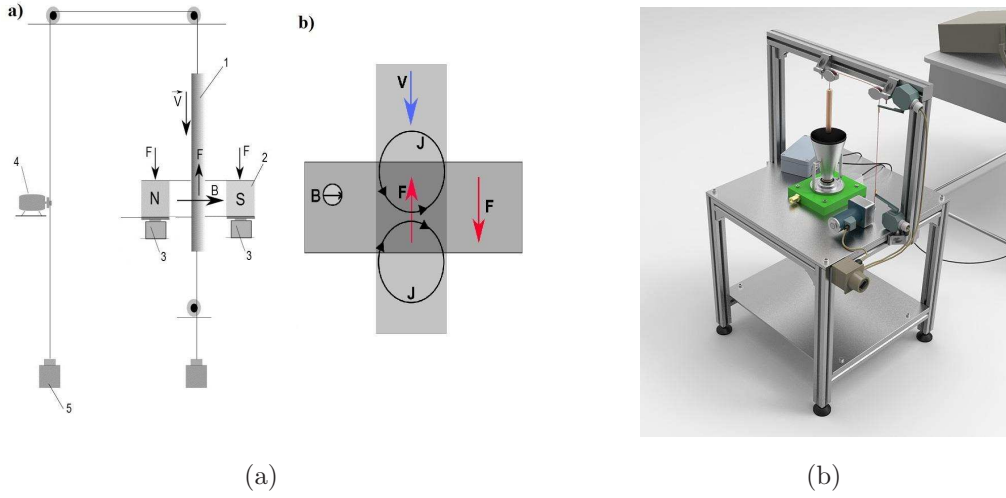


Figure 4.5: 2D and 3D schematic of Lorentz force sigmometry setup for conductivity measurements of solid metals after adding some technical modifications to the LOFOS used for fluid measurements. (a) 2D schematic of Lorentz force sigmometry setup for electrical conductivity measurements of solid metals. 1: sample of a solid metal; 2: Halbach magnet; 3: force sensor; 4: Mdlar motor; 5: weight. (b) 3D schematic of Lorentz force sigmometry setup for electrical conductivity measurements of solid metals.

When the motor is switched on, the 30 cm rod (Fig. 4.5a , pos. 1) moves through the magnetic field of the Halbach magnet with a linear speed of 10 cm s^{-1} . The bar needs 3s to pass through the magnetic field. By increasing the Lorentz force, the magnet acts on the sensor. When the bar exits the magnetic field, the stop element automatically turns the motor off. During the experiment, the Lorentz force and temperature near the force sensor were continuously measured. During the 3s exposure of the solid bar to the magnetic field, eddy currents were generated inside the metal (Fig. 3.4b). By Ampere's law, the eddy currents give rise to a secondary magnetic field. As a result, the Lorentz force acts to slow the movement of the solid bar and, owing to Newton's third law, a measurable force equal to the Lorentz force acts upon the magnet. This force is directly proportional to the electrical conductivity of the solid bar. The force acting on the magnet presses the strain gauge sensor located beneath the magnet system. The signal from the sensor, after being processed by the second and third device (see Fig. 3.3), is fed to a voltmeter and then to the computer defining the Lorentz force F and force integral \tilde{F} within the operating time. The density ρ is measured by calculating the volume V and the mass M of the bar, using the equation $\rho = \frac{M}{V}$. We conducted two series of measurements. The first measurements were used to determine the calibration factor of the given LOFOS geometry with the

copper and aluminum cylindrical bars; the electrical conductivity of the bars had been previously measured with the help of a commercial device using the eddy current testing method called SigmaTest 2.069. This commercial device has a wide measuring range, 0.5 MS to 65 MS, with an absolute accuracy of $\pm 0.5\%$, as well as five selectable operating frequencies; we used an operating frequency of 60 kHz, for which the resolution was equal to 0.1% of the measured value. The second measurements were conducted with a brass bar to determine its electrical conductivity using the calibration factor obtained in the first experiment. To calculate the statical error of the electrical conductivity using the Lorentz force sigmometry method, we measured the electrical conductivity of the brass bar using the SigmaTest device and compared it with that measured by LOFOS.

4.3 Determination of calibration factor using copper and aluminum bars

In this section, we discuss the conductivity measurements of the copper and aluminum bars. The goal of these experiments was to determine the calibration factor, K , which can be calculated after transformation of Eq. 3.6 as follows:

$$K = \frac{\sigma M}{\rho \tilde{F}} \quad (4.1)$$

Both bars (copper and aluminum) had a length of $L = 299.5 \pm 0.7$ mm [using Eq. 3.11 from section 3.7] and diameter $\varnothing = 9.98 \pm 0.02$ mm.

Their electrical conductivities, σ , were measured by a commercial device, SigmaTest, based on the eddy current testing method. We connected its probe to the surfaces of the bars and recorded the values; these experiments were repeated ten times at room temperature (20 °C). Subsequently, the mean values of the measurements were calculated as $\sigma_{cu} = 58.106$ MS m⁻¹ and $\sigma_{al} = 21.698$ MS m⁻¹. If we add the standard deviation for copper and aluminum then the electrical conductivity of copper is $\sigma_{cu} = 58.106 \pm 0.29$ MS m⁻¹ and for aluminum is $\sigma_{al} = 21.698 \pm 0.11$ MS m⁻¹.

As we mentioned before, the interaction time between the bar and the magnetic field was 3 s. We repeated the measurements several times over several days.

4.3.1 Copper measurements

Here, we present selected results as an example for copper measurements:

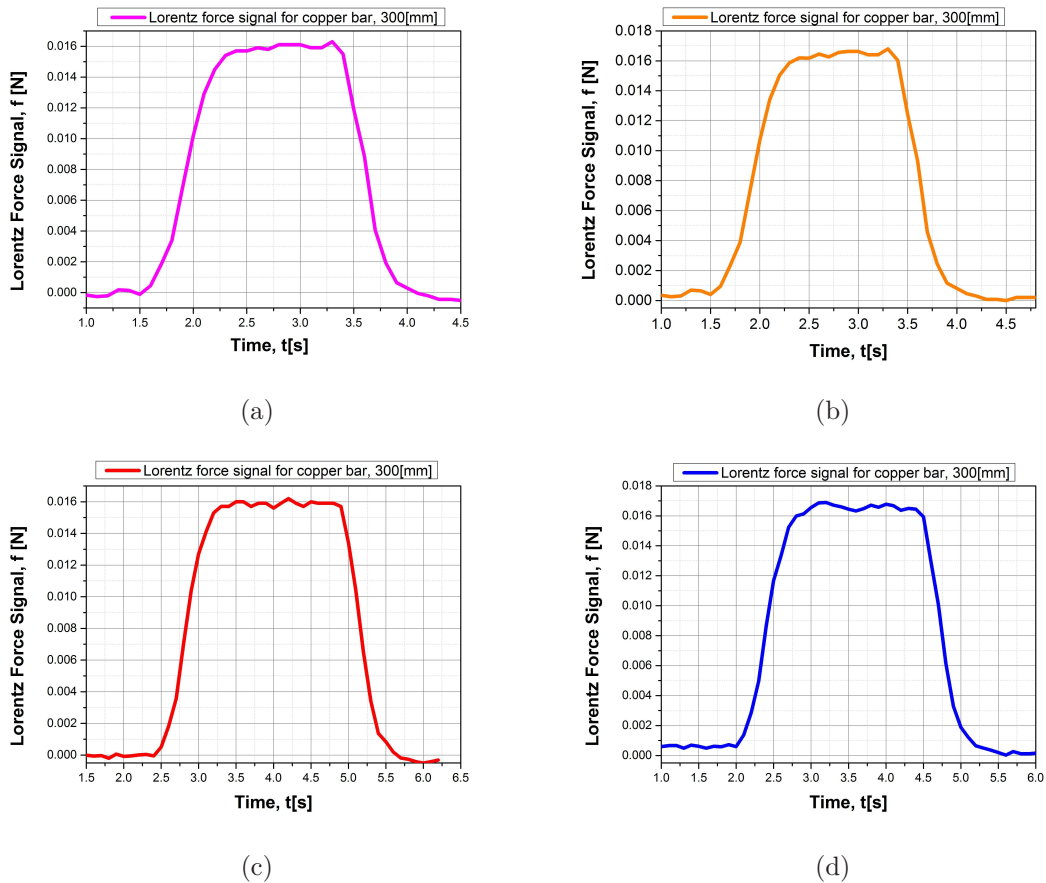


Figure 4.6: Lorentz force signal for the copper bar shows that the Lorentz force equals zero when the copper bar is outside the magnetic field. It then increases to its maximum value and remains constant for some seconds before the bar leaves the magnetic field, at which point the Lorentz force returns to zero.

Figure 4.6 shows that when the bar is outside the magnetic field, the Lorentz force is equal to zero; then, when the bar passes through the magnetic field, the force increases and remains stable for a few seconds, depending on the linear speed of the motor and the length of the solid bar. When the whole bar has passed through the magnetic field, the force becomes zero again. The magnitude of the force is ~ 0.016 N and its integral equals to 0.0372 Ns. Notably, these are raw signals obtained directly from the source; no filter has been applied to them. The motor had two directions of movement (up and down). We recorded the Lorentz force also in the other direction, as shown in Fig 4.7.

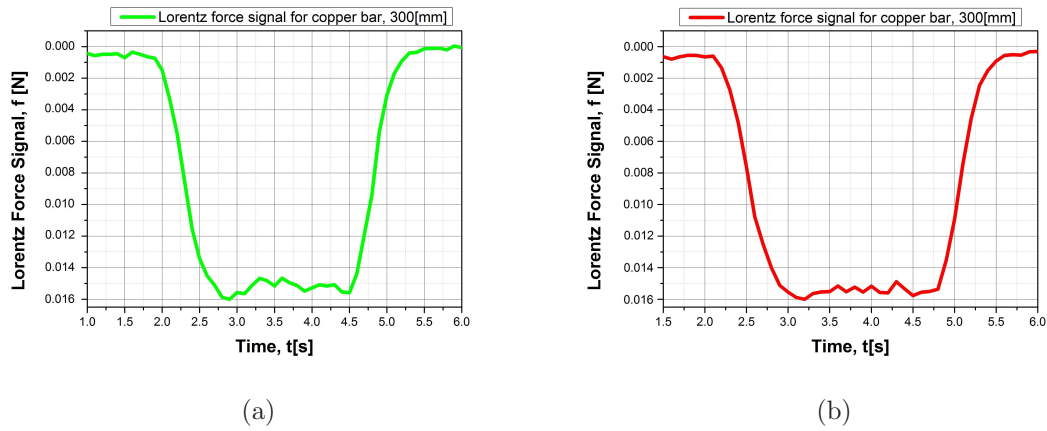


Figure 4.7: Lorentz force signal for copper bar when it passes the magnetic field in the opposite direction. These curves shows the same behavior but in the opposite direction.

We noticed that the amplitude of the Lorentz force was smaller in this direction because the velocity was not equal to the one in the up direction. A slower velocity led to slower amplitude of Lorentz force as it is proportional to the linear velocity of the conductor. Figure 4.7 shows the integration of the Lorentz force signal between t_1 and t_2 ; where t_1 is the time when the conductive bar starts to interact with magnetic field and it equals as an example to 1.5s in Fig. 4.6 in the upper right orange curve and t_2 is when the bar leaves the area of magnetic field and t equals as an example to 4s in the same orange curve. However, we use for calculating the integral a commercial program named "Origin 9.0G". This program use the trapezoidal rule to approximate the definite integral. Trapezoidal Rule is based on the Newton-Cotes Formula that states if one can approximate the integrand as an n th order polynomial [Abramowitz & Stegun, 1965]. The integral of Lorentz force equals to 0.0372 ± 0.001 [N s].

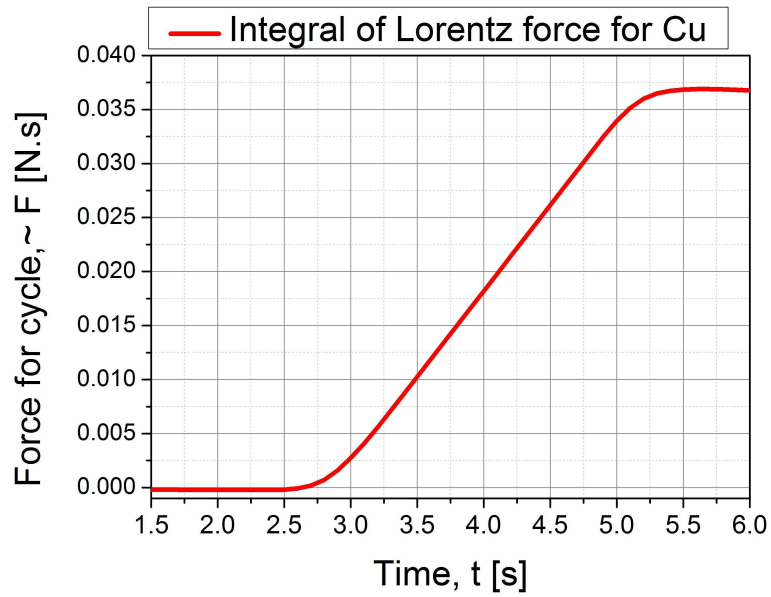
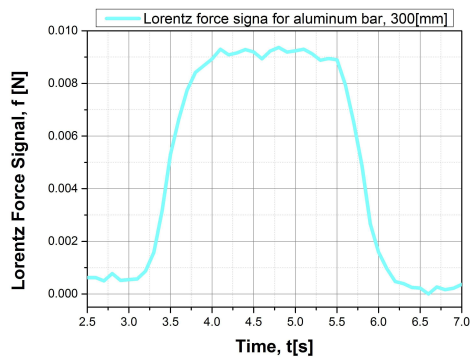


Figure 4.8: Integral of Lorentz force for copper bar between t_1 and t_2 , which is the time period during which the copper bar interacts with the magnetic field, moving up case.

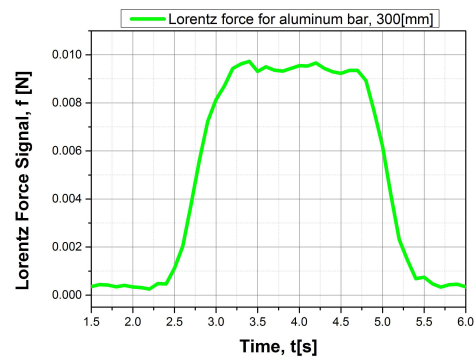
4.3.2 Aluminum measurements

We repeated the same experiment with an aluminum bar in both directions. Figure 4.9 shows the same behavior as for the copper bar. We notice that the Lorentz force amplitude is smaller as compared to the Lorentz force of the copper bar. This is because the conductivity of aluminum is smaller than that for copper. The Lorentz force is ~ 0.009 N .

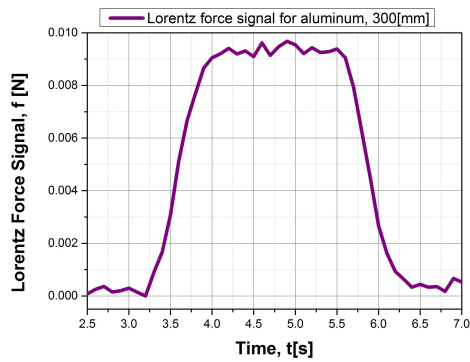
4. Electrical Conductivity Measurements of Solid Metals



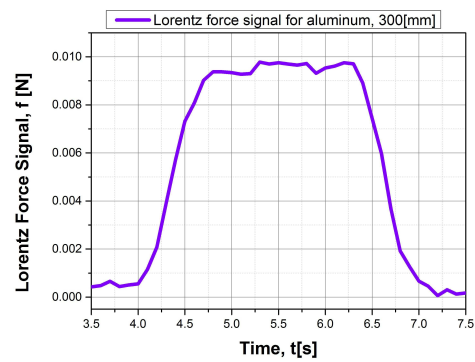
(a)



(b)



(c)



(d)

Figure 4.9: The Lorentz force signal for the aluminum bar shows that the Lorentz force equals to zero when the aluminum bar is outside the magnetic field. It increases to a maximum value and remains constant for some seconds. When the bar leaves the magnetic, the Lorentz force returns to zero.

We notice the same behavior in the opposite direction: a smaller amplitude of Lorentz force signal for the aluminum bar.

4. Electrical Conductivity Measurements of Solid Metals

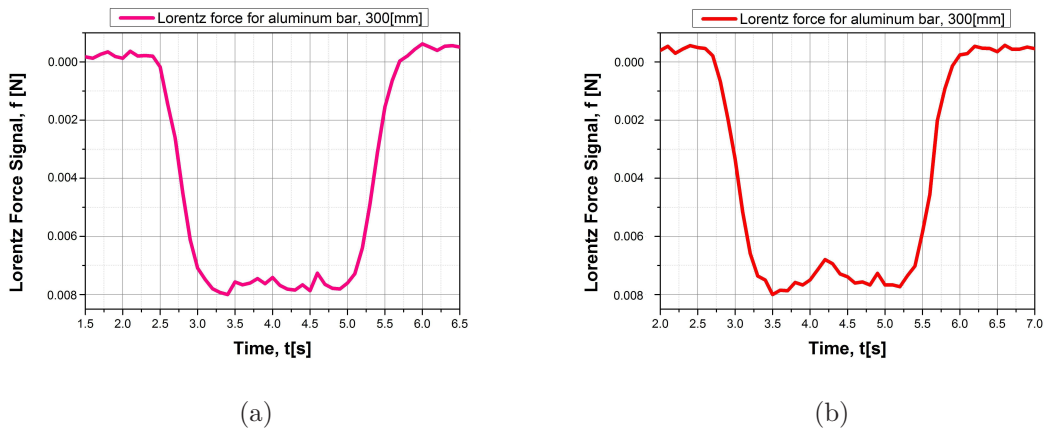


Figure 4.10: The Lorentz force signal for the aluminum bar when it passes the magnetic field in opposite direction. These curves show the same behavior but in the opposite direction.

The integral of the Lorentz force is 0.0214 ± 0.0003 [N s]:

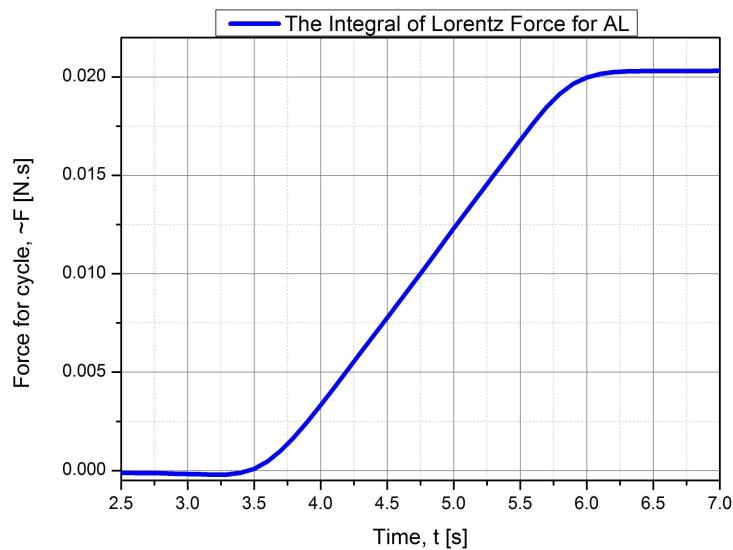


Figure 4.11: Integral of the Lorentz force for the aluminum bar between t_1 and t_2 , which is the time period during which the aluminum bar interacts with the magnetic field.

Equation 4.1 was used to calculate the calibration factor of the device (see Tab.4.1).

A small difference is observed between the calibration factors obtained from copper and aluminum. This difference can be attributed to the uncertainty measurements of the calibration factor. We decided to use the mean value of the

4. Electrical Conductivity Measurements of Solid Metals

Table 4.1: Calculation of the calibration factor K from copper and aluminum measurements

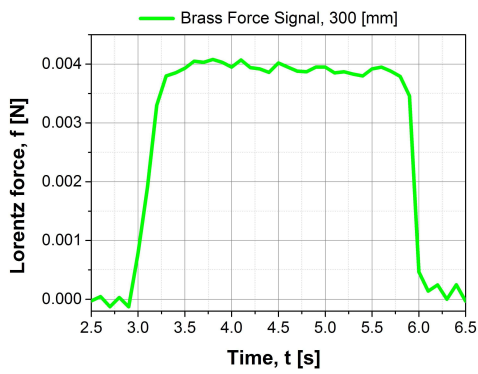
Material	σ [MS m ⁻¹]	Mass [g]	Density [$\frac{\text{kg}}{\text{m}^3}$]	\tilde{F} [Ns]	\mathbf{K} [$\frac{\text{m}^2\text{S}}{\text{Ns}}$]
Copper	58.106 \pm 0.29	195.02 \pm 0.023	8935.3 \pm 55.3	0.0372 \pm 0.001	34094.9 \pm 1295.6
Aluminum	21.698 \pm 0.11	59.16 \pm 0.031	2786.7 \pm 15.6	0.0214 \pm 0.0003	34637 \pm 845.14

calibration factor from copper and aluminum measurements to determine the electrical conductivity of brass, as the calibration factor should not depend on the type of material. The mean value of the calibration factor is 34366 $\frac{\text{m}^2\text{S}}{\text{Ns}}$.

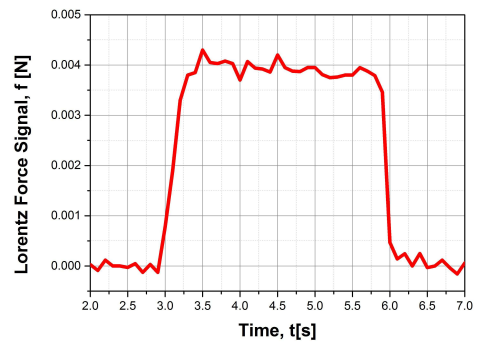
4.4 Electrical conductivity measurement of brass bar

To prove that the Lorentz force sigmometry device can measure the electrical conductivity of solid metals, we prepared a brass bar with the same geometry as the copper and aluminum bars and repeated the same measurement procedure.

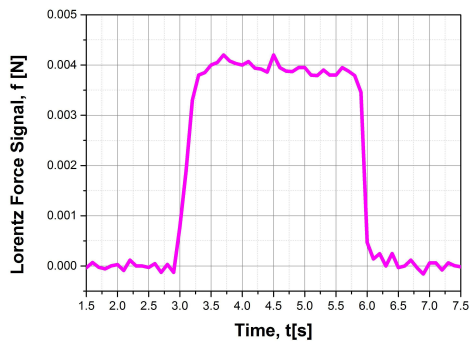
4. Electrical Conductivity Measurements of Solid Metals



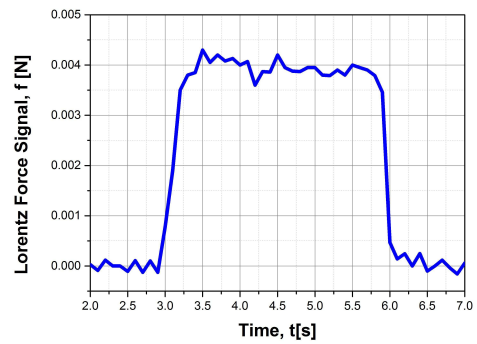
(a)



(b)



(c)



(d)

Figure 4.12: Lorentz force signal for brass bar shows that Lorentz force equals to zero when the copper bar is outside the magnetic field area and then it rises to its maximum and keep constant for some seconds before the bar leaves the magnetic area and goes back to zero again.

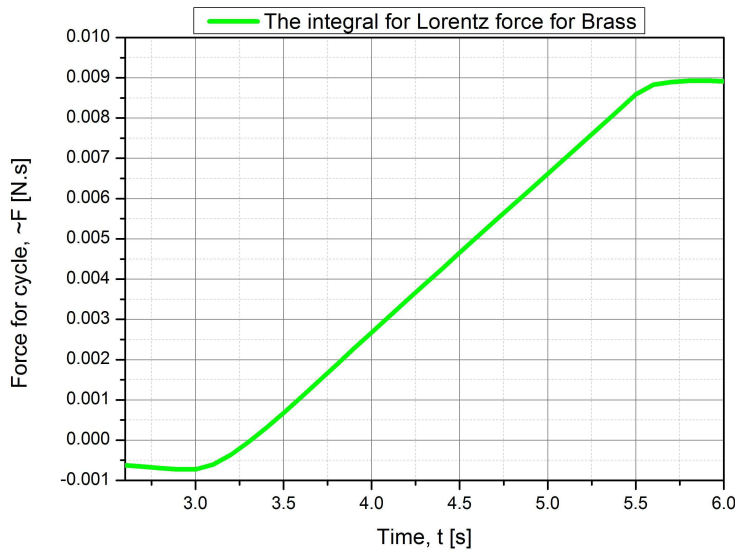


Figure 4.13: Integral of Lorentz force for brass bar between t_1 and t_2 which is the time period that brass bar interacts with the magnetic field.

To calculate the electrical conductivity, we used Eq. 3.6 and adopted the mean value of the calibration factor obtained from the first series of measurements.

Table 4.2: Calculation of the electrical conductivity of brass bar

\mathbf{K} [$\frac{\text{m}^2\text{S}}{\text{N}\cdot\text{s}}$]	\mathbf{Mass} [g]	ρ [$\frac{\text{kg}}{\text{m}^3}$]	$\tilde{\mathbf{F}}$ [N s]	σ [MS m^{-1}]
34366 ± 383.3	187.47 ± 0.025	8376.6 ± 44.3	0.00892 ± 0.0001	13.75 ± 0.38

As reported in Tab.4.2, the electrical conductivity for brass was equal to 13.75 ± 0.38 [MS m^{-1}], as measured by the Lorentz force sigmometry method. To check the statistical error of our result, we measured the electrical conductivity of the brass bar ten times using the commercial device SigmaTest at room temperature, and then calculated the mean value of the ten measurements. This value was equal to 14.03 ± 0.21 MS m^{-1} . The difference between the values obtained with the two methods is very small and the possibility of error was 1.9%; this result ensures that the Lorentz force sigmometry method is able to measure the electrical conductivity of solid metals. Figure 4.14 shows the Lorentz force signals for the three metal bars. High electrical conductivity metals, such as copper, have a strong effect on the magnetic system, and vice versa; low electrical conductivity metals, like brass, affect the magnets with a low force. After finishing the experiments with solid metals, we investigated the fluids.

4. Electrical Conductivity Measurements of Solid Metals

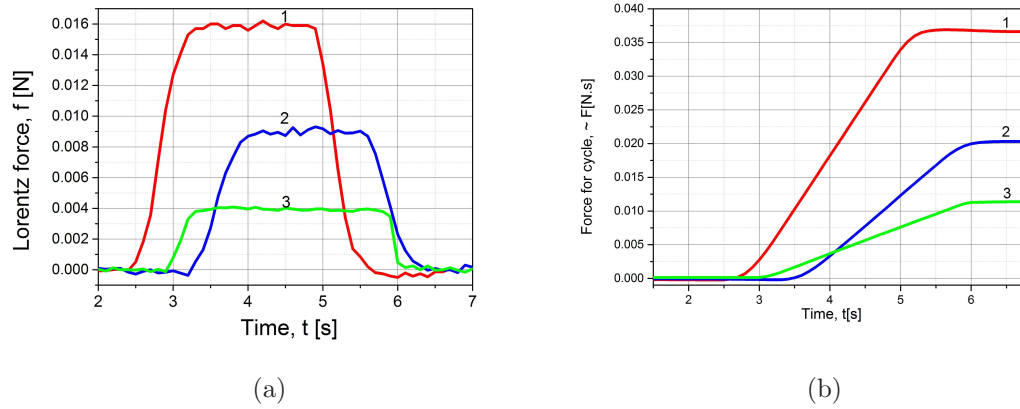


Figure 4.14: Figure comparing the Lorentz force signal for the three bars that were measured in the lab. The curves show that high electrical conductivity metals (copper) have a strong effect on the magnetic system and vice versa; low electrical conductivity metals, such as brass, affect the magnets with a low force. (a) Lorentz force signal for copper (1, red), aluminum (2, blue), and brass (3, green) bars. (b) Integral of Lorentz force for cycle, $\sim F$ [N.s] for copper (1, red), aluminum (2, blue), and brass (3, green) bars

Chapter 5

Electrical conductivity measurements of molten metals

In this chapter, we present the results obtained using the Lorentz force sismometry setup for fluid measurements. After explaining the procedure of measurements in section 5.1.1, we calibrate the device using the known physical properties of a eutectic alloy named galinstan, GaInSn, in order to find the calibration factor, K , of the setup, which is necessary to calculate the electrical conductivity of molten metals using Lorentz force sismometry. This is explained in detail in section 5.1.2. After knowing the calibration factor, we repeat the measurement with the unknown electrical conductivity of molten tin at different temperatures and compare our results with the reference values in section 5.2.

5.1 Calibration factor calculation using eutectic alloy GaInSn

The goal of this experiment was to find the calibration factor K of the device by using the known physical properties of an alloy with the composition of $Ga^{67}In^{20.5}Sn^{12.5}$. This is a eutectic alloy at room temperature and its melting temperature is $T_m = 10.5^\circ\text{C}$. For fluid measurements, we fabricated a special quartz conical vessel capable of withstanding temperatures ranging from room temperature up to 1000°C . The nozzle had a diameter of 8 mm and it allowed

the flow of molten metal across the magnet system during some seconds, which is reasonable for measuring the Lorentz force with good accuracy.

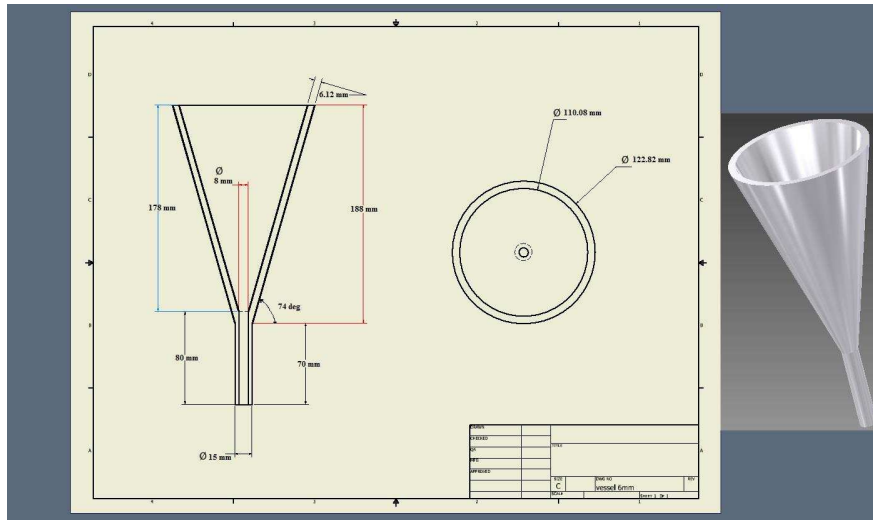


Figure 5.1: 3D schematic of the Lorentz force sismometry setup for fluid measurements. 1: filling funnel; 2: Halbach magnet and force sensor; 3: collecting vessel; 4: electronic scale; 5: amplifier and converter; 6: voltmeters; 7: computer; 8: transformer and converter.

The dependence of physical properties such as density and electrical conductivity on the temperature is determined by: $\rho = 6492.12 - 0.44T$ [kg m^{-3}] and $\sigma = 1/(R_0 T [0.9632 + 2.9 \times 10^{-3}])$ where $R_0 = 30.32 \times 10^{-8}$ [Ωm]. We have this formula from Russian federal state research and design institute of rare metal industry GIREDMET, who analysis the physical properties of this special alloy at different temperatures (see appendix for details).

Because the nozzle geometry of the filling funnel for fluid measurements was smaller than that of the funnel used for solid measurements, a new calibration factor was necessary for an accurate fluid measurement.

5.1.1 Measurements procedure

The setup for this experiment was explained in detail in a previous chapter (section 3.2). We repeat the figure in this section so the reader can follow the procedure better.

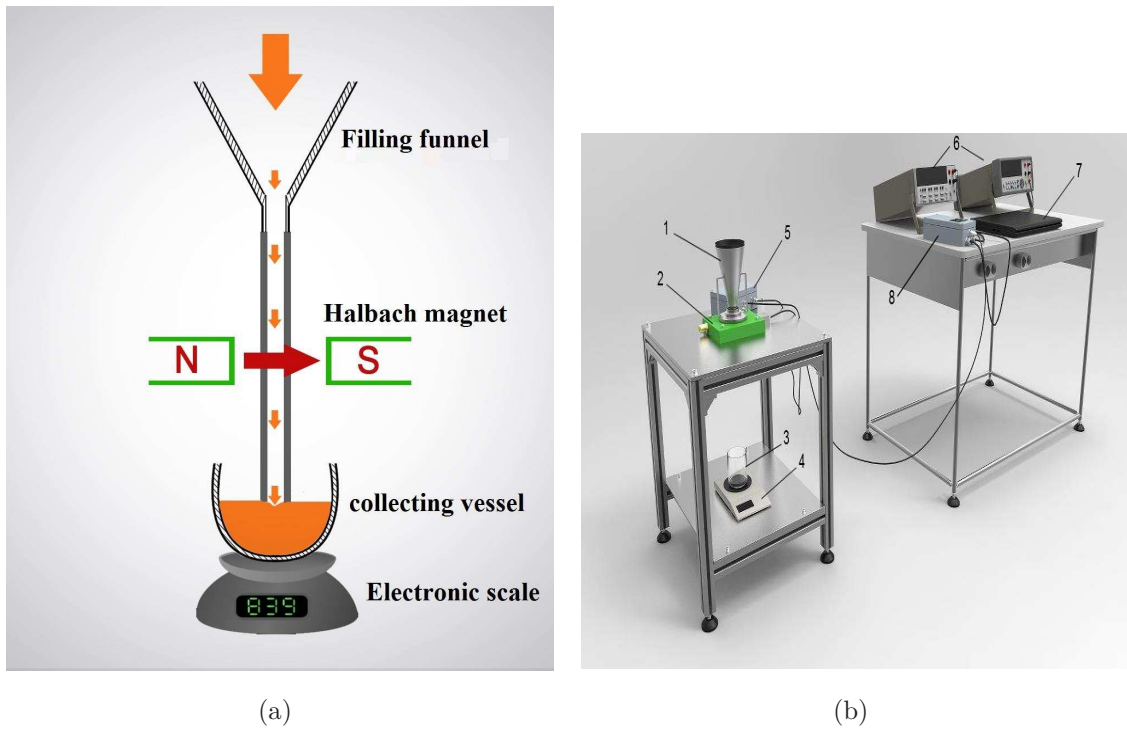


Figure 5.2: (a) Principle sketch of Lorentz force sismometry. The molten metal is poured into a filling funnel and then projected through a magnetic field generated by the cylindrical Halbach magnet. (b) 3D schematic of the Lorentz force sismometry setup for fluid measurements. 1: filling funnel; 2: Halbach magnet and force sensor; 3: collecting vessel; 4: electronic scale; 5: amplifier and converter; 6: voltmeters; 7: computer; 8: transformer and converter.

A vessel with the volume $V = 600 \text{ mL}$ is filled with galinstan alloy. Before beginning the experiment, an empty vessel with the volume of 1 L is placed on the scale platform under the LOFOS nozzle, as shown in Fig. 5.2b.

The experimental procedure is as follows: first, we measure the temperature of the eutectic alloy before each experiment, and then pour the alloy into the filling funnel (Fig. 5.2b, pos.1) placed above the LOFOS device. The liquid metal under gravitation force penetrates in the LOFOS device (Fig. 5.2b, pos.2) passing through the nozzle in the presence of a magnetic field.

The interaction of the metal flow with the magnetic field generates the Lorentz force in the molten metal in a direction opposite to that of the flow, and induces force acting on the magnet system directed along the flow, which is exactly equal to Lorentz force in the liquid metal. The molten metal passing through the LOFOS setup is accumulated in the collecting vessel (Fig. 5.2b, pos.3) placed on the platform of the electronic scale (Fig. 5.2b, pos.4) for the direct determination of the cumulative mass M . The scale is connected to a computer (Fig. 5.2b, pos.7),

and special software is used for the mass measurement during the process. The force acting on the magnet presses the sensor located underneath the magnet system. The signal from the sensor is fed to a commercial voltmeter (Fig. 5.2b, pos.6), and then to a computer determining the Lorentz force F and its integral \tilde{F} within the operating time $\Delta t = t_2 - t_1$.

5.1.2 Lorentz force signal of galinstan alloy

In this section, we present some examples of the measurements with galinstan. We did more than 80 experiments in total and then we calculate the mean value of the calibration factor of all this experiments. Here are some selected signals of Lorentz force measurements of galinstan alloy.

5. Electrical Conductivity Measurements of Molten Metals

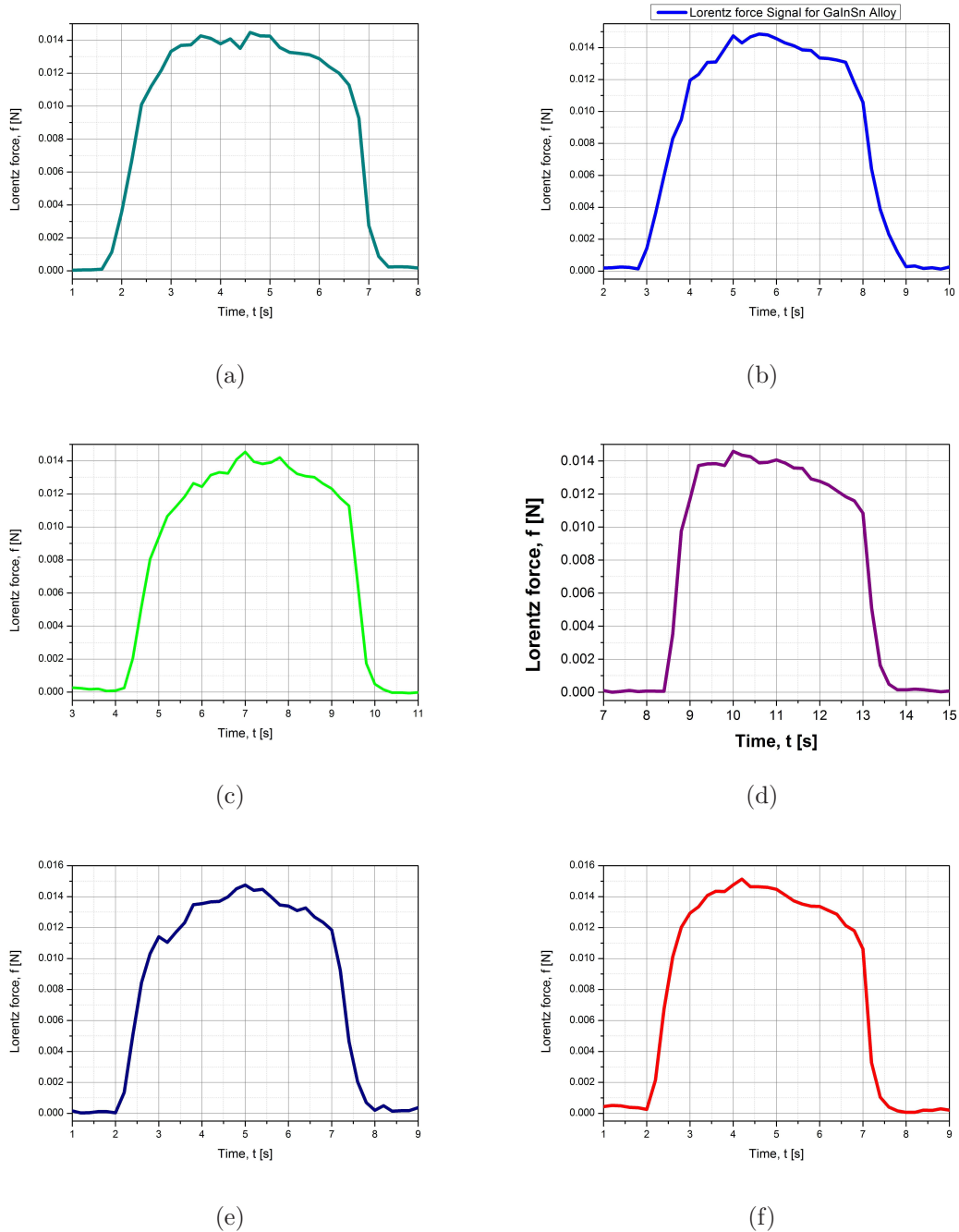


Figure 5.3: The Lorentz force signal for galinstan alloy shows that the Lorentz force equals zero when the copper bar is outside the magnetic field, and then it increases to its maximum and remains constant for some seconds before the bar leaves the magnetic area, at which time the Lorentz force returns to zero.

Figure 5.3 shows the same behavior for the Lorentz force. When the conducting fluid is outside the magnetic field, the Lorentz force equals zero; it then increases during the interaction and remains stable for ~ 5 second. It then returns to

5. Electrical Conductivity Measurements of Molten Metals

zero when the conducting fluid leaves the magnetic field. For calculating the calibration factor, we use the integral of the Lorentz force(Fig. 5.4)

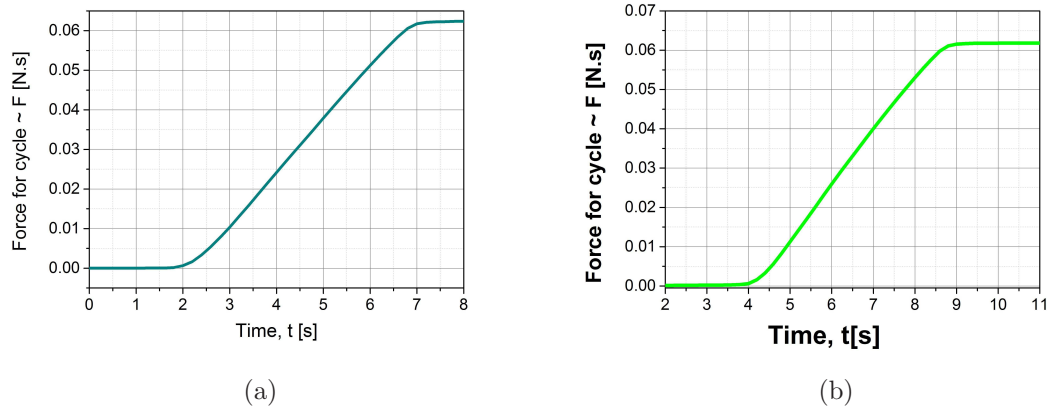


Figure 5.4: Integral of Lorentz force for galinstan alloy between t_1 and t_2 , which is the time period during which the eutectic alloy interacts with the magnetic field.

Next figure shows the histogram diagram of the calibration factor that we measured using galinstan alloy:

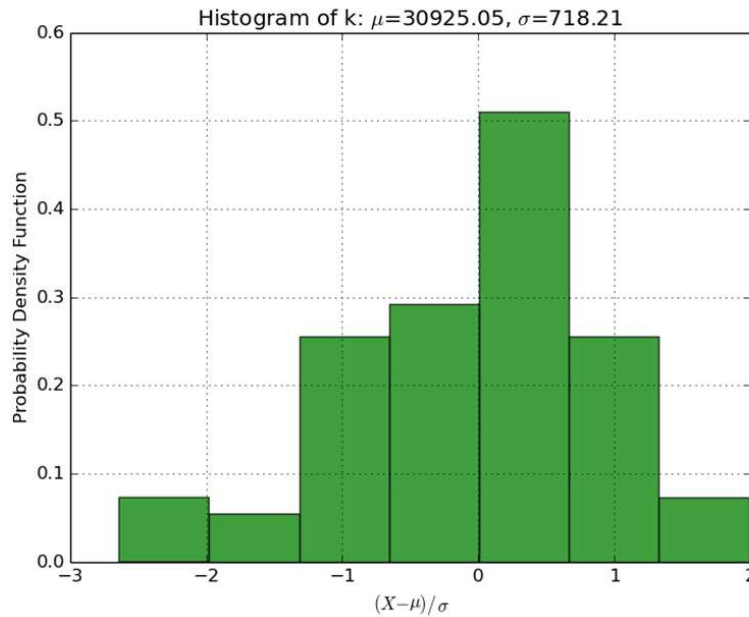


Figure 5.5: Histogram diagram of the calibration factor K of 83 measurements using galinstan alloy.

The mean value for the calibration factor calculated from the measurements with

its standard deviation is $30925 \pm 718 \frac{\text{m}^2\text{S}}{\text{Ns}}$. After finding the new calibration factor for the fluid measurements, a molten metal with unknown electrical conductivity could be investigated. We chose to start with molten tin because it has a low melting temperature of $T_m = 232^\circ\text{C}$, which is suitable for doing experiments in lab environment.

5.2 Electrical conductivity measurement of molten tin

We used the same setup as the one for galinstan, but because we were working with a high-temperature liquid metal, we needed to use an air compressor pump to cool the area around the magnet and the force measurement systems, as shown in Figs. 5.5 a,b and Figs. 5.6 a, b.

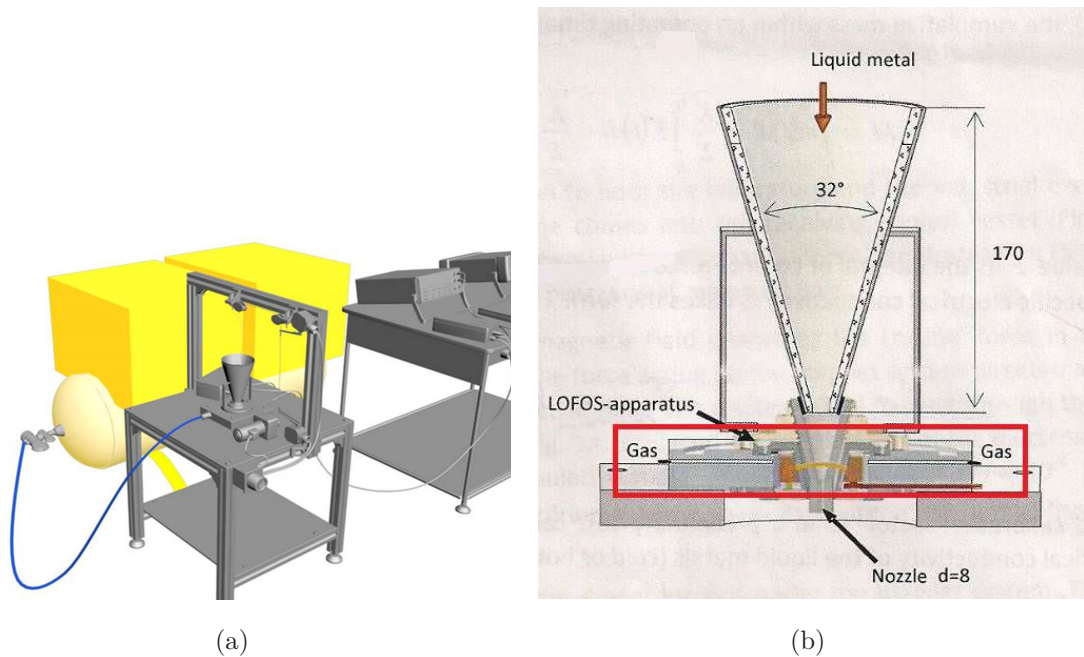


Figure 5.6: (a) 3D setup of Lorentz force sigmometry shows the air compressor pump connected to the main setup. (b) Cross section of Lorentz force sigmometry shows the inlet and outlet of the air to cool the area around the magnet and force sensor systems.



Figure 5.7: (a) Photograph of the air compressor pump used in the lab. (b) Photograph of the other end of the cable that connect the air compressor pump to the LOFOS setup.

The procedure for this experiment was as follows:

- The tin (with 9.99% purity) was melted to ~ 250 °C.
- The quartz vessel was preheated to decrease variation in the tin temperature during the measurement.
- The temperature of the tin was measured before pouring it into the vessel to assure the fast response of the sensor during the measurements.
- The cooling system was turned on to keep the temperature low and stable in the magnetic field area.
- The liquid was poured and the Lorentz force recorded. The cumulative mass of the metal was read to calculate the electrical conductivity.
- The quartz vessel was cleaned to avoid changing the geometry of the vessel nozzle for the second measurement.

In our first test with molten tin, we faced significant solidification (see Fig. 5.8) because the temperature of the molten tin was in the range of the melting temperature of the tin, $T_m = 232$ °C.

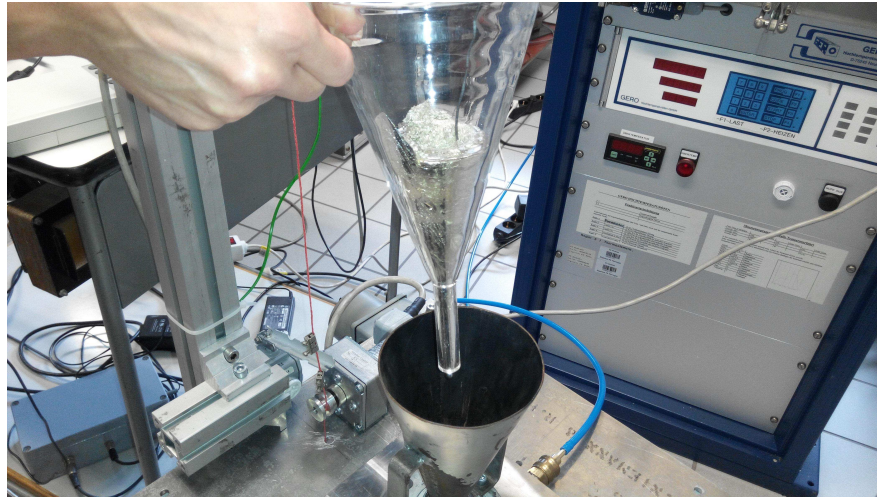


Figure 5.8: Photograph showing significant solidification of molten tin in the quartz vessel when the molten temperature was close to the melting temperature of the tin.

However, we were able to resolve this issue by increasing the temperature of the alloy above the melting point ($> 232\text{ }^{\circ}\text{C}$ for tin) ($\sim 350\text{ }^{\circ}\text{C}$) and by preheating the quartz funnel longer using an air heater ($\sim 610\text{ }^{\circ}\text{C}$). As a result, we overcame the problem of solidification, and we observed that the nozzle walls were free of any solidified tin after each measurement.

We recorded the Lorentz force signal for the tin. The next figure shows some of these measurements.

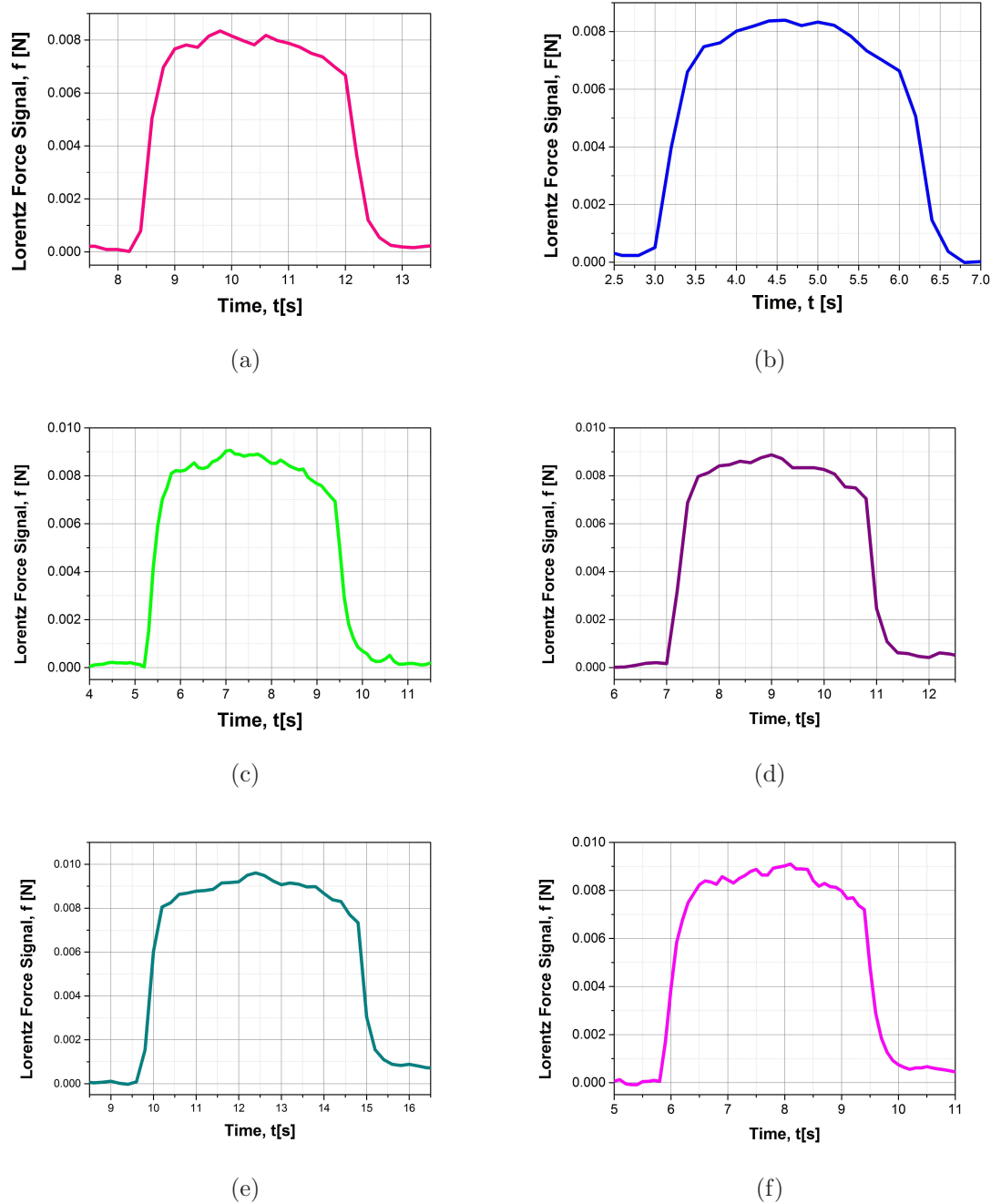


Figure 5.9: The Lorentz force signal for molten tin shows that the Lorentz force equals zero when the molten tin is outside the magnetic field. It then increases to its maximum value and remains constant for some seconds before the molten tin leaves the magnetic field, at which point the Lorentz force returns to zero.

Some measurements were affected by mechanical noise from the compressor during the experiment, as shown in Fig. 5.10.

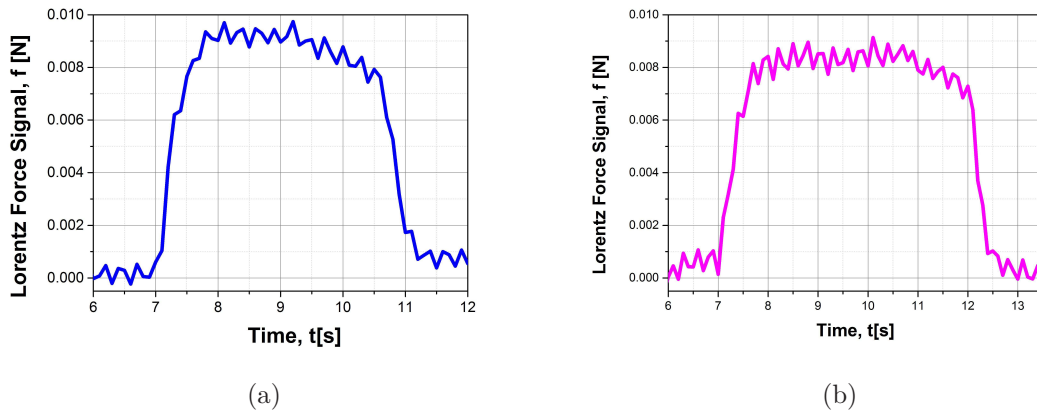


Figure 5.10: Lorentz force signal of molten tin when it suffers form mechanical noise.

We know from chapter 3.1 that the formula to calculate the electrical conductivity is given as:

$$\sigma = \rho K \frac{\tilde{F}}{M} \quad (5.1)$$

Thus, we needed to know the density of the molten tin, which depends on the temperature of the alloy. We used the following formula to calculate the density of tin at different temperatures [Alchagirov & Chochaeva, 1998] :

$$\rho = 7374.7 - (676.5 \times 10^{-3}T) \quad (5.2)$$

where ρ is the density of tin in kg m^{-3} and T is the temperature of molten tin in kelvin. Alchagirov & Chochaeva [1998] claimed an error of 0.05%.

We calculated the integral of the Lorentz force as shown in Fig. 5.11 . We noticed that for different measurements of molten tin, we had different integrals of the Lorentz force because of different temperatures.

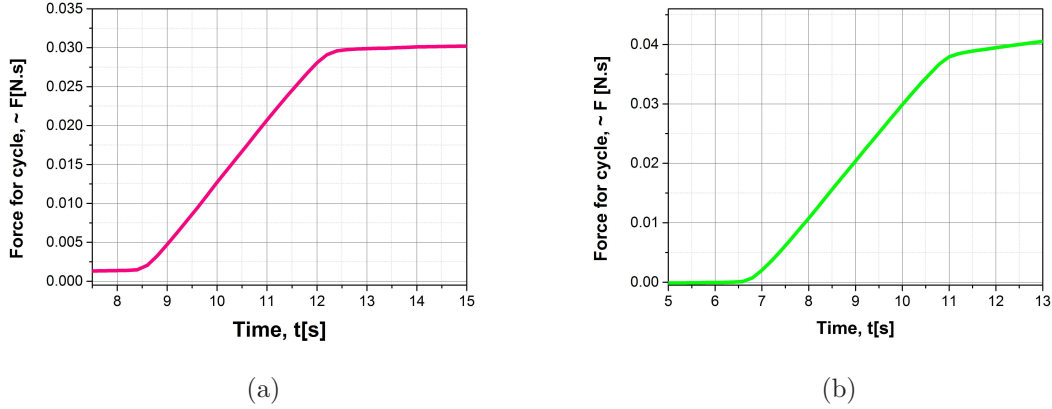


Figure 5.11: Integral of Lorentz force signal of molten tin at different temperatures..

We calculated the electrical conductivity of molten tin at different temperatures. However, when we compared our results with other methods, we noticed a significant statistical error, which ranged from $\sim 8 - 20\%$.

We repeated the measurements without the cooling system and obtained better results. However, they were not as good as we expected because the temperature near the magnetic system was high. This changed the magnetic field, such that the calibration factor was inversely proportional to the square of the magnetic field (see Eq. 3.3).

This effect was investigated by Kolesnikov et al. in their LFF prototype. They used commercial rare-earth permanent magnets consisting of NdFeB to characterize the dependence of their magnetization on temperature. They found that the magnetic induction decreased by 8.5 % when the temperature of the magnets increased from 293 K to 363 K (20 °C to 90 °C) [Kolesnikov *et al.*, 2011]. In particular, the dependence was calculated according to the following equation:

$$B(T_M) = B_0[(1 - \alpha(T_M - T_{0M}))] \quad (5.3)$$

where B_0 is the magnetic field induction at the initial magnet temperature $T_{0M} = 293 \text{ K}$ and α is the coefficient of temperature variation of the magnetic field and it equals to $\alpha = 1.116 \times 10^{-3} [\text{K}^{-1}]$.

Because using the cooling system was necessary in high-temperature measurements, we decided to re-calibrate the device using galinstan alloy when the air compressor pump was on.

Following the same steps mentioned above in section 5.1.2 , we found the new calibration factor of the device, which was equal to $27258 \pm 806 \frac{\text{m}^2\text{S}}{\text{N}_s}$

We repeated the measurements with molten tin at different temperatures and then compared our results with those in the literature. Figures (5.12 and 5.13) show the comparison between our measurements with the LOFOS setup and those from the literature, taking into account the uncertainty of force measurements. The uncertainty of temperature measurement ΔT is estimated to be as high as 1.1°C . We use thermocouple type K and its uncertainty for temperature range 0°C to 1250°C has been analyzed by Nakos [2004]. The following temperature-dependent correlations have been reported for the resistivity of molten tin using contact methods (electrodes) of 99.95% molten tin [Roll & Motz, 2000; Scala & Robertson, 1953; Sharafat & Ghoniem, 2000]:

For $T < 588.15\text{ K}$

$$R(T) = 40.88 + 0.0272T \quad (5.4)$$

For $T > 588.15\text{ K}$

$$R(T) = 41.16 + 0.0263T \quad (5.5)$$

where $R(T)$ [$\mu\Omega\text{ cm}$] is the resistivity of molten tin at temperature T [K].

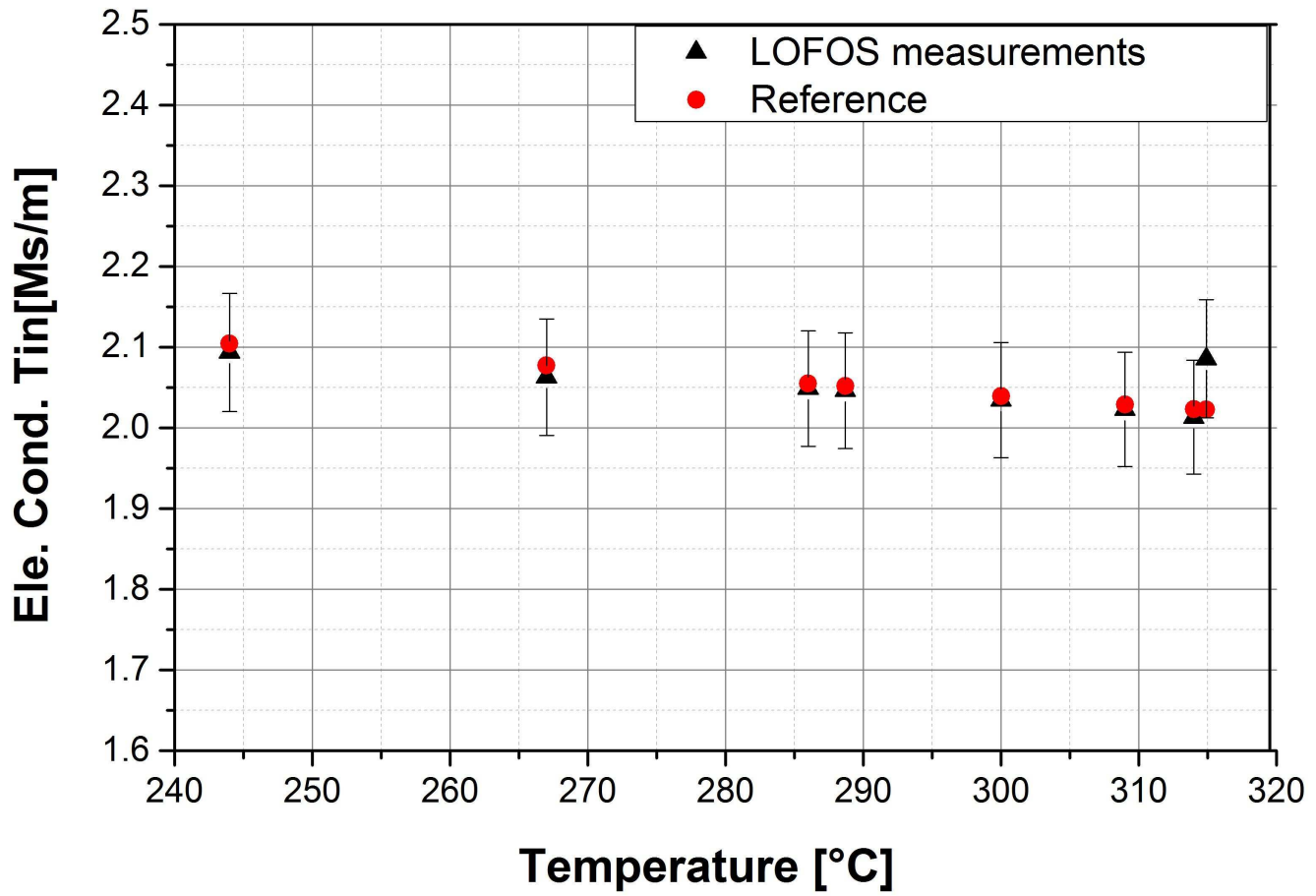


Figure 5.12: Dependence of electrical conductivity of molten tin at temperatures below 315°C using the Lorentz force sigmometry method and literature results.

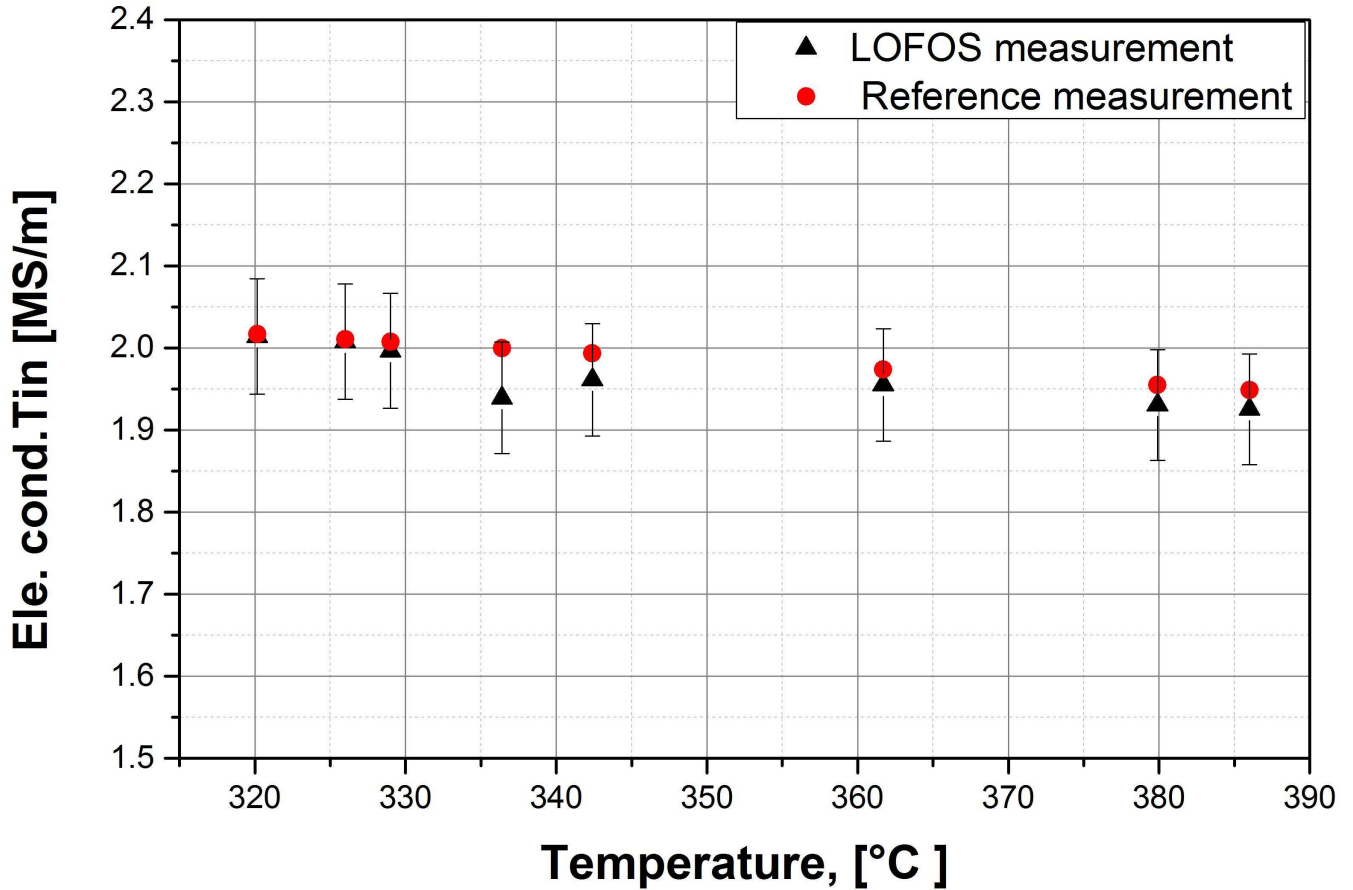


Figure 5.13: Dependence of electrical conductivity of molten tin at temperatures greater than 315 °C using the Lorentz force sigmometry method and literature results.

Figures (5.12 and 5.13) show that the electrical conductivity decreased with increasing temperature. The reason for this decrease can be explained as follows. The conductivity of a material depends directly on both the number of free electrons per unit volume, n , and on the average time between collisions, τ . As we increased the temperature, the average speed of the electrons, which act as the carriers of current, increased, resulting in more frequent collisions. The average time of collisions, τ , thus decreased with increasing temperature, which decreased the conductivity of the metals. As a result of all measurements using LOFOS, we noticed an error of as much as 6% as compared to the literature values. However, the literature don't show their uncertainty to be an accurate comparisons. This type of error called statistical error (see section 3.7) which express the precision of the used measurement method. Unfortunately, for hot liquid measurements, we

couldn't estimate the standard deviation so the random error for mass and force. The reason for that is the complicated control of molten tin temperature in the lab. Even if we measure the temperature before pouring the liquid through the nozzle, the temperature will vary during pouring according to the temperature of the quartz vessel and the weather condition. A good solution for this problem is to fix a vacuum induction melting furnace over the quartz vessel and isolated the whole setup to prevent temperature variation. Thus, a repetition of measurements with the same temperature can be possible. However, we can estimate the random error as following: we know that 0.4% error is coming from temperature measurements and 0.05% is from the density measurements [Alchagirov & Chochaeva, 1998] and 3% from calibration factor measurements with galinstan rise the relative random error in this measurements to 3.45%.

The total error (statistical and random) of molten measurements is less than 10%.

Chapter 6

Conclusion and Outlook

Lorentz force sigmometry is a non-contact electrical conductivity measurement method based on the principles of magnetohydrodynamics. Because of the interaction of an externally applied magnetic field with a moving electrical conductor, eddy currents within the conductor lead to a Lorentz force, which drags the magnetic field-generating system along the flow direction. This force linearly depends on the electrical conductivity of the conductor and can be measured using an accurate force sensor.

Accurate measurements of the physical properties of aggressive and hot molten metals is crucial for proper optimization and control over metallurgical processes such as continuous casting and powder production. Up to today, these factors have been known in metallurgy with an uncertainty higher than 10%. Out of all these properties, the electrical conductivity is of particular interest because it helps in increasing the quality of the finished products.

This thesis describes the design and laboratory tests of a Lorentz force sigmometry mobile device for solid and liquid metals. The method has the following advantages: i) because there is no direct contact between the sensor and the sample, it can be implemented in the production process of any non-magnetic material (e.g. copper or aluminum); (ii) it is based on simple theory and involves a simple setup; (iii) the LOFOS setup is portable and easy to move; (iv) a relatively short period is required for the measurement (3–5 s is sufficient). The circular shape of the Halbach magnet does not limit the penetration depth, which is usually limited to a few micrometers in conventional eddy current methods. The described contactless method is applicable to the measurement of the electrical conductivity of all the common high-temperature non-ferromagnetic molten metals, including

refractory metals.

Conclusion: Electrical conductivity measurements of solid metals

We conducted two series of experiments with cylindrical solid bars. The first was with known electrical conductive bars made of aluminum and copper (length 150 mm, diameter 10 mm) to compute the calibration factor of the device, K . This calibration factor was then used to estimate the unknown electrical conductivity of a brass bar with the same geometry. Our results show an uncertainty of as much as 5%. This uncertainty is the sum of the random error and the statistical error of electrical conductivity measurements.

Conclusion: Electrical conductivity measurements of molten metals

This experiment was done with molten metals. The first series was carried out with an alloy with known physical properties having the composition of $Ga^{67}In^{20.5}Sn^{12.5}$. This is a eutectic alloy at room temperature and its melting temperature is $T_m = 10.5^\circ\text{C}$. The aim of these measurements was to find the new calibration factor, K , of the special quartz filling funnel, which was fabricated to sustain temperatures ranging from room temperature up to 1000°C . The nozzle has a diameter of 8 mm, and it allowed the flow of molten metal across the magnet system during a $\Delta t \approx 5.5$ [s], which is reasonable for measuring the Lorentz force with good accuracy.

The second series of experiments were with high-temperature molten tin $T_m = 232^\circ\text{C}$. For fluid measurements, in order to protect the LOFOS force measurement system from high temperatures, we added an external air compressor pump to the LOFOS setup and re-calibrated the device when the cooling system was on because we found that keeping the temperature near the magnet system at room temperature was crucial for good results. Then, we compared the LOFOS results with those reported in the literature. The comparison showed an uncertainty of as much as 6% for temperature range smaller and bigger than 315°C . A total uncertainty (statistical and random error) of these measurements is less than 10%.

Outlook

Lorentz force sismometry can measure the electrical conductivity of solid and molten metals using a very simple concept with good accuracy. We can use this novel device to build a vast database of different alloys and solid metals that can

6. Conclusion and Outlook

be used in industry for increasing the quality of finished products. Two other configurations of the LOFOS setup can be built and tested to measure the density and viscosity of molten metals in future.

Appendix

6.1 Physical properties of galinstan alloy

This analysis has been done in Russian federal state research and design institute of rare metal industry "GIREDMET".

1. Alloy compositions

It is a eutectic alloy made of gallium 67% , Indium 20.5 % and Tin 12.5 %.

2. Melting temperature

The melting temperature of galinstan alloy is $T_m = 10.5^\circ\text{C}$.

3. Density of alloy in dependence with temperature

After accurate analysis of the density of galinstan alloy with temperatures in the range 298.15 K to 523.15 K, they found this formula:

$$\rho = 6492.12 - 0.44T \text{ [kg m}^{-3}\text{]}.$$

Table 6.1: The density of galinstan alloy in dependence with temperature

Temperature [K]	Density [kg m ⁻³]
298.15	6360.934
323.15	6349.934
348.15	6338.934
373.15	6827.934
398.15	6316.934
423.15	6305.934
448.15	9294.934
473.15	6283.934
498.15	6272.934
523.15	6261.934

4. Electrical resistivity of alloy in dependence with temperature

An analysis of the electrical resistivity of galinstan alloy with temperatures in the range 298.15 K to 523.15 K, gives this formula:

$$R[T] = R_0 T [0.9632 + 2.9 \times 10^{-3}]$$

where $R_0 = 30.32 \times 10^{-8} [\Omega \text{ m}]$.

Table 6.2: The electrical resistivity of galinstan alloy in dependence with temperature

Temperature [K]	Electrical resistivity $\times 10^{-8} [\Omega \text{ m}]$
298.15	3.058
323.15	3.278
348.15	3.498
373.15	3.718
398.15	3.938
423.15	4.157
448.15	4.377
473.15	4.597
498.15	4.817
523.15	5.037

6.2 Data sheet of strain gauge sensor

In the LOFOS force measurement system, we use a strain gauge which made by Japanese company named Tokyo Sokki Kenkyujo Co., Ltd.

TML strain gauge test data

- Gauge type: UFLA-1-350-23 - Gauge factor: $2.15 \pm 1\%$ - Test condition: 23°C 50% RH
- Gauge resistance: $350 \sim 1.0 \Omega$
- Temperature coefficient of G. F. : $+0.08 \pm 0.05 \%/10^\circ\text{C}$
- Coefficient of thermal expansion: $23.0 \times 10^{-6}/^\circ\text{C}$

Next figure shows the relation of thermal output (apparent strain) with temperature:

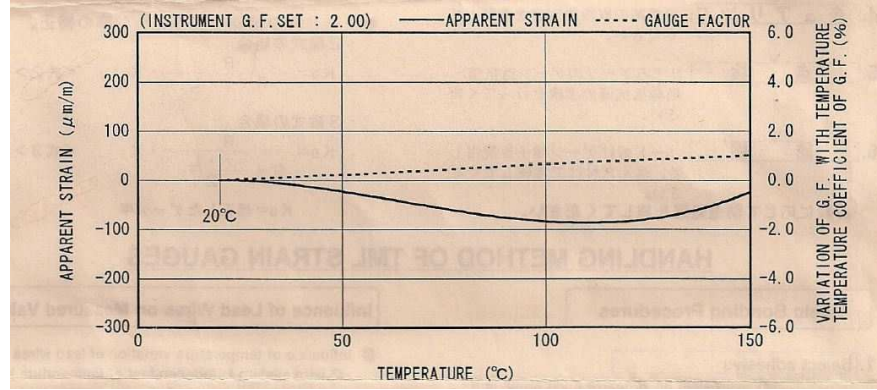


Figure 6.1: Apparent strain Vs. temperature

Influence of lead wires on measured values

A. Influence of temperature variation of lead wires (3-wire system is independent of temperature).

$$\varepsilon_l = \frac{rL\alpha\Delta T}{K(R + rL)} \quad (6.1)$$

where ε_l is the thermal output of lead wires, r is total resistance per meter of lead wires $\Omega \text{ m}^{-1}$, L is the length of the lead wires m , α is the temperature coefficient of resistance of lead wires, K is gauge factor and R is the gauge resistance.

B. Gauge factor correction due to lead wire attachment in case of 2-wire system

$$K_0 = \frac{R}{R + r \cdot L} \cdot K \quad (6.2)$$

In case of 3-wire system

$$K_0 = \frac{R}{R + \frac{r \cdot L}{2}} \cdot K \quad (6.3)$$

where K_0 corrected gauge factor.

List of Figures

List of Figures

1.1	Continuous casting process of steel. (a) Manufacturing process of continuous casting of steel in industry (courtesy of Vizag Steel). (b) Continuous casting process. 1: Ladle. 2: Stopper. 3: Tundish. 4: Shroud. 5: Mold. 6: Roll support. 7: Turning zone. 8: Shroud. 9: Bath level. 10: Meniscus. 11: Withdrawal unit. 12: Slab. A: Liquid metal. B: Solidified metal. C: Slag. D: Water-cooled copper plates. E: Refractory material (courtesy of Wikipedia). . .	3
1.2	Schematic of the working principle of Lorentz force velocimetry. (a) A moving electrically conductive fluid is exposed to a magnetic field. (b) An eddy current is induced inside the fluid by the external magnetic field. (c) The eddy current induces a secondary magnetic field. (d) The interaction of the magnetic field with the eddy current generates a Lorentz force (braking force) on the fluid. Then, owing to Newton’s third law, a force equal to the Lorentz force acts on the magnet, which can be measured using a force sensor.	4
2.1	Two-probe method for measuring the electrical conductivity of a conductor. It consists of an AM meter to measure the current in the specimen and a voltmeter to measure the potential difference between the two ends of the long parallel pipe-shaped sample. . .	9
2.2	Four-probe method for measuring the electrical conductivity of a conductor. It consists of four equally spaced tungsten metal probes and two voltmeters (courtesy of Wikipedia).	10
2.3	The Wheatstone bridge (direct current DC) consists of four resistances consists of four impedance.	11
2.4	The Wheatstone bridge [alternating current (AC)].	12
2.5	Electrical conductivity measurement using the eddy current method (courtesy of Victor Aviation).	13

List of Figures

2.6	Normalized impedance curves for planar circular coil varying with reference numbers r/δ (coil radius/skin depth) and lift-off (coil-to-sample spacing)[Ma & Peyton, 2006].	15
2.7	The four-probe method for electrical conductivity measurement of molten metal consists of two current electrodes, two potential electrodes, and one thermocouple.	17
2.8	Principle of electromagnetic levitation. The rf magnetic levitation field induces eddy currents in the sample which, together with the field, generate Lorentz forces that support the sample against gravity [Lohoefer, 2005].	18
2.9	Schematics of electromagnetic levitation: the droplet is placed in an alternating magnetic field inside a radiofrequency current carried on the primary coil. The induced voltage in the secondary coil depends on the electrical conductivity of the sample.	19
2.10	Picture of a hot electromagnetically levitated sample enclosed by the alternating current carrying levitation coil on the ground. The coil consists of a copper tube which is cooled from within by running water. The upper counterwinding prevents the lateral escape of the sample (courtesy of DLR-MP).	20
2.11	Inductive method using rotating magnetic field for measuring the electrical conductivity. It consists of a rotating magnetic field and a molten metal (sample) suspended by a rope and located inside the magnetic field. It measures the electrical conductivity of the sample by measuring the torque.	21
3.1	Two-dimensional (2D) schematic of the Lorentz force sismometry setup for measuring the electrical conductivity of molten metals. 1: filling funnel, 2: Halbach magnet, 3: collecting vessel, and 4: electronic scale.	25
3.2	Three-dimensional (3D) schematic of the Lorentz force sismometry setup for measuring the electrical conductivity of molten metals. 1: filling funnel, 2: LOFOS-apparatus, 3: collecting vessel, 4: electronic scale, 5: amplifier and converter, 6: voltmeters, 7: computer, and 8: transformer and converter.	26
3.3	LOFOS-apparatus diagram; 1: Circular Halbach magnet and force sensor, 2: thermocouple sensor, 3: amplifier and converter, 4: converter and transformer, 5: voltmeter, 6: computer.	27

3.4	(a) Two-dimensional (2D) schematic of Lorentz Force Sigmometry setup for electrical conductivity measurements of solid metals. 1: sample of a solid metal, 2: Halbach magnet, 3: force sensor, 4: Madler motor, 5: weight. (b) A braking force acts on the conducting bar and is matched by an accelerating force on the magnet.	28
3.5	Solid metals setup: three-dimensional (3D) schematic of Lorentz force sigmometry setup for measuring the electrical conductivity of solid metals; it consists of 1- sample of a solid material, 2- filling funnel, 3- LOFOS-apparatus, 4- amplifier and converter, 5- Madler motor, 6- stop elements, 7- voltmeters, 8- computer, 9- transformer and converter.	29
3.6	A zoom in of 3D schematic of Lorentz force sigmometry showing the Halbach cylinder surrounding the nozzle of the filling funnel.	30
3.7	FEM model of cylindrical Halbach array with 8 magnets. The colored domains indicate the magnitude of the magnetic induction. [Weidermann, 2013].	31
3.8	(a) Cross section of cylindrical Halbach magnet in x–y plane shows the radii, R_i and R_o for the inner and outer circles, respectively. (b) Optimization of Lorentz force generation using Halbach cylinder magnet system. Three magnetization patterns with 8, 12, and 16 trapezoidal segments [Weidermann, 2013].	32
3.9	Ferromagnetic cylinder showing various magnetization patterns and magnetic fields. The red box refers to the type used in the current Lorentz force sigmometry setup. (courtesy of Wikipedia).	32
3.10	Magnetic field distribution in the inner space of the Halbach magnet. The arrows show the magnetization direction of the magnet elements.	33
3.11	Design of the magnet system. a) The top view shows the diameters of the inner and outer circles and b) the single magnet segment. c) Three-dimensional schematic of the Halbach cylinder.	33

List of Figures

3.12	Influence of ferromagnetic materials on the magnetic field distribution. (a) Dependence of the transversal component of the magnetic field from the axial coordinate along the symmetry axis of the magnet system itself, as well as for the magnet system if installed in the nozzle holder plate, which is shown in (b). (c) Dependence of the transversal component of the magnetic field from the axial coordinate along the symmetry axis for the magnet system installed in the nozzle holder plate under the additional influence of the ferromagnetic iron block at a distance h from the bottom edge of the nozzle holder plate [shown in (d)].	34
3.13	Photo of Halbach cylinder magnet system picture. It shows its different; parts housing lower part, housing top and the twelve symmetrically aligned trapezoidal permanent magnets.	34
3.14	A sketch explaining the working principle of the strain gauge under exaggerated bending (courtesy of Wikipedia).	35
3.15	Bridge strain gauge circuit (courtesy of Allaboutcircuit website).	36
3.16	Photograph of the force measurement system of the Lorentz force sigmometry, which consisted of three bridge strain gauge circuits working as one sensor to measure the Lorentz force of the moving conductive material.	37
3.17	Photograph of force measurement system of Lorentz force sigmometry during installation.	37
3.18	Photo of force measurement system calibration of Lorentz force sigmometry. This photo shows a weight equals to 50 g over the measurement system.	38
3.19	Linear fit of force sensor measurements in volt using LOFOS with the reference values in newton in order to calculate the slope which equals to the calibration factor.	39
4.1	Three cylindrical bars made of copper(red), aluminum(gray) and brass(yellow). They have identical dimensions: $L = 150$ mm and $Q = 10$ mm. (taken with a camera).	44
4.2	Illustration of the first test experiment. The solid bar is accelerated by gravity and passes the magnetic field lines with a velocity of 0.2 m s^{-1} .The Lorentz force acts to slow the conductor movement, while simultaneously another force equal to the Lorentz force acts on the magnet.	44

4.3	Lorentz force signal for copper bar when it passes the magnetic field with gravity acceleration (free-fall velocity).	45
4.4	Lorentz force signal for copper bar when it passes the magnetic field with gravity acceleration (free-fall velocity). It is a single peak signal because the orientation of the bar as it passed through the magnetic field was incorrect.	46
4.5	2D and 3D schematic of Lorentz force sigmometry setup for conductivity measurements of solid metals after adding some technical modifications to the LOFOS used for fluid measurements. (a) 2D schematic of Lorentz force sigmometry setup for electrical conductivity measurements of solid metals. 1: sample of a solid metal; 2: Halbach magnet; 3: force sensor; 4: Mdlar motor; 5: weight. (b) 3D schematic of Lorentz force sigmometry setup for electrical conductivity measurements of solid metals.	47
4.6	Lorentz force signal for the copper bar shows that the Lorentz force equals zero when the copper bar is outside the magnetic field. It then increases to its maximum value and remains constant for some seconds before the bar leaves the magnetic field, at which point the Lorentz force returns to zero.	49
4.7	Lorentz force signal for copper bar when it passes the magnetic field in the opposite direction. These curves shows the same behavior but in the opposite direction.	50
4.8	Integral of Lorentz force for copper bar between t_1 and t_2 , which is the time period during which the copper bar interacts with the magnetic field, moving up case.	51
4.9	The Lorentz force signal for the aluminum bar shows that the Lorentz force equals to zero when the aluminum bar is outside the magnetic field. It increases to a maximum value and remains constant for some seconds. When the bar leaves the magnetic, the Lorentz force returns to zero.	52
4.10	The Lorentz force signal for the aluminum bar when it passes the magnetic field in opposite direction. These curves shows the same behavior but in the opposite direction.	53
4.11	Integral of the Lorentz force for the aluminum bar between t_1 and t_2 , which is the time period during which the aluminum bar interacts with the magnetic field.	53

List of Figures

4.12	Lorentz force signal for brass bar shows that Lorentz force equals to zero when the copper bar is outside the magnetic field area and then it rises to its maximum and keep constant for some seconds before the bar leaves the magnetic area and goes back to zero again.	55
4.13	Integral of Lorentz force for brass bar between t_1 and t_2 which is the time period that brass bar interacts with the magnetic field.	56
4.14	Figure comparing the Lorentz force signal for the three bars that were measured in the lab. The curves show that high electrical conductivity metals (copper) have a strong effect on the magnetic system and vice versa; low electrical conductivity metals, such as brass, affect the magnets with a low force. (a) Lorentz force signal for copper (1, red), aluminum (2, blue), and brass (3, green) bars. (b) Integral of Lorentz force for copper (1, red), aluminum (2, blue), and brass (3, green) bars	57
5.1	3D schematic of the Lorentz force sigmometry setup for fluid measurements.1: filling funnel; 2: Halbach magnet and force sensor; 3: collecting vessel; 4: electronic scale; 5: amplifier and converter; 6: voltmeters; 7: computer; 8: transformer and converter.	60
5.2	(a) Principle sketch of Lorentz force sigmometry. The molten metal is poured into a filling funnel and then projected through a magnetic field generated by the cylindrical Halbach magnet. (b) 3D schematic of the Lorentz force sigmometry setup for fluid measurements.1: filling funnel; 2: Halbach magnet and force sensor; 3: collecting vessel; 4: electronic scale; 5: amplifier and converter; 6: voltmeters; 7: computer; 8: transformer and converter.	61
5.3	The Lorentz force signal for galinstan alloy shows that the Lorentz force equals zero when the copper bar is outside the magnetic field, and then it increases to its maximum and remains constant for some seconds before the bar leaves the magnetic area, at which time the Lorentz force returns to zero.	63
5.4	Integral of Lorentz force for galinstan alloy between t_1 and t_2 , which is the time period during which the eutectic alloy interacts with the magnetic field.	64
5.5	Histogram diagram of the calibration factor K of 83 measurements using galinstan alloy.	64

5.6	(a) 3D setup of Lorentz force sigmometry shows the air compressor pump connected to the main setup. (b) Cross section of Lorentz force sigmometry shows the inlet and outlet of the air to cool the area around the magnet and force sensor systems.	65
5.7	(a) Photograph of the air compressor pump used in the lab. (b) Photograph of the other end of the cable that connect the air compressor pump to the LOFOS setup.	66
5.8	Photograph showing significant solidification of molten tin in the quartz vessel when the molten temperature was close to the melting temperature of the tin.	67
5.9	The Lorentz force signal for molten tin shows that the Lorentz force equals zero when the molten tin is outside the magnetic field. It then increases to its maximum value and remains constant for some seconds before the molten tin leaves the magnetic field, at which point the Lorentz force returns to zero.	68
5.10	Lorentz force signal of molten tin when it suffers form mechanical noise.	69
5.11	Integral of Lorentz force signal of molten tin at different temperatures.. . . .	70
5.12	Dependence of electrical conductivity of molten tin at temperatures below 315°C using the Lorentz force sigmometry method and literature results.	72
5.13	Dependence of electrical conductivity of molten tin at temperatures greater than 315°C using the Lorentz force sigmometry method and literature results.	73
6.1	Apparent strain Vs. temperature	81

REFERENCES

References

- ABRAMOWITZ, MILTON & STEGUN, IRENE A. 1965 *Handbook of Mathematical Functions*. Dover Publications, INC., New York.
- ALCHAGIROV, B. B. & CHOCHAEVA, A. M. 1998 Temperature dependence of the density of liquid tin. *HIGH TEMPERATURE* **38**.
- ALKHALIL, SHATHA, THESS, ANDR & KOLESNIKOV, YURII 2015 Lorentz force sigmometry: a novel technique for measuring the electrical conductivity of solid and liquid metals. *Measurement Science and Technology* **26**.
- BAKER, ROGER C. 2000 *Flow Measurement Handbook*. Cambridge University Press.
- BAKHITYAROV, S. I. & OVERFELT, R. A. 1999 Electrical conductivity measurements in liquid metals by rotational technique. *Journal of Material Science* **34**, 945–949.
- BEAN, C. P., DEBLOIS, R. W. & NESBITT, L. B. 1959 Eddy current method for measuring the resistivity of metals. *Journal of Applied Physics* **30**.
- BLAIR, M. & STEVENS, T.L. 1995 *Steel Casting Handbook*. Steel Founders Society of America and ASM International.
- BOWLER, NICOLA & HUANG, YONGQIANG 2005a Electrical conductivity measurement of metal plates using broadband eddy-current and four-point methods. *MEASUREMENT SCIENCE AND TECHNOLOGY* **16**.
- BOWLER, NICOLA & HUANG, YONGQIANG 2005b Electrical conductivity measurement of metal plates using broadband eddy-current and four-point methods. *MEASUREMENT SCIENCE AND TECHNOLOGY* **16**.
- BRAUNBEK, WERNER 1932 Eine neue methode elektrodenloser leitfähigkeitsmessung [in german]. *Zeitschrift fr Physik* **73**, 312–334.

REFERENCES

- BRODOVA, I. G., POPEL, P. S. & ESKIN, G.I. 2002 *Liquid Metal Processing*. Taylor and Francis.
- CHABERSKI, A. Z. 1971 Contactless induction method for electric resistivity measurement. *Journal of Applied Physics* **42** (3), 940–947.
- C.MARANGONI 1878 Sul principio della viscosita superficiale dei liquidi stabilito dal sig. j. plateau. *Nuovo Cimento* pp. 97–115.
- CONSOLIVER, EARL & MITCHELL, GROVER 1920 *Automotive ignition systems*. New York, McGraw-Hill.
- DELANEY, J. A. & PIPPA, A. B. 1972 Electrodeless methods for conductivity measurement in metals. *Rep. Prog. Phys.* .
- DODD, C. V. & DEEDS, W. E. 1968 Analytical solutions to eddy-current probe-coil problems. *Journal of Applied Physics* **39** (6).
- EDMONDS, A. R. 1996 *Angular Momentum in Quantum Mechanics*. Princeton University Press.
- EGRY, I. 2004 Physical property measurements of liquid metals at high temperatures under microgravity. *Materials Transactions* **45**, 3235–3240.
- GRANT, I. S. & PHILLIPS, W. R. 1990 *Electromagnetism*, 2nd edn. Wiley.
- JENSEN, K. D. 2004 Flow measurements. *Journal of the Brazilian Society of Mechanical Sciences and Engineering* **4**.
- KEITHLEY 2005 Measuring the resistivity and determining the conductivity type of semiconductor materials using a four-point collinear probe and the model 6221 dc and ac current source. *Keithley Instruments, Inc.* .
- KOLESNIKOV, YURII, KARCHER, CHRISTIAN & THESS, ANDR 2011 Lorentz force flowmeter for liquid aluminum: Laboratory experiments and plant tests. *Metallurgical and Materials Transactions B* **42** (3), 441–450, 10.1007/s11663-011-9477-6.
- LARK-HOROVITZ, K. & JOHNSON, VIVIAN A. 1959 *Solid State Physics*, 6th edn. ACADEMIC PRESS New York and London.
- LOHOEFER, G. 2005 Electrical resistivity measurement of liquid metals. *Measurement Science and Technology* pp. 417–425.

-
- MA, X. & PEYTON, A. J. 2006 Eddy current measurement of the electrical conductivity and porosity of metal foams. *IEEE transactions on instrumentation and measurement* **55** (2).
- MICCOLI, I., EDLER, F., PFNUER, H. & TEGENKAMP, C. 2015 The 100th anniversary of the four-point probe technique: the role of probe geometries in isotropic and anisotropic systems. *Journal of Physics: Condensed Matter* **27**.
- MONAGHAN, B. J. 1999 A four-probe dc method for measuring the electrical resistivities of molten metals. *International Journal of Thermophysics* **20** (2).
- NAKOS, JAMES T. 2004 Uncertainty analysis of thermocouple measurements used in normal and abnormal thermal environment experiments at sandias radiant heat facility and lurance canyon burn site. *Sandia National Laboratories* .
- PHYSIKALISCH-TECHNISCHE BUNDESANSTALT 2006 Gravity Information System.
- PLEVACHUK, Y., SKLYARCHUK, V., HOYER, W. & KABAN, I. 2006 Electrical conductivity, thermoelectric power and viscosity of liquid sn-based alloys. *Journal of Materials Science* **41**, 4632–4635.
- PLEVACHUK, Y., SKLYARCHUK, V., YAKYMOVYCH, A., ECKERT, S., WILLERS, B. & EIGENFELD, K. 2008 Density, viscosity, and electrical conductivity of hypoeutectic al-cu liquid alloys. *Metallurgic and Materials Transactions A* **39A**, 3040–3045.
- PRIEDE, J., BUCHENAU, D. & GERBETH, G. 2011 Contactless electromagnetic phase-shift flow meter for liquid metals. *Measurement Science and Technology* **22**.
- RICHARDSEN, T., LOHFER, G. & EGRY, I. 2002 Electrical resistivity of undercooled liquid cu-ni alloys. *International Journal of Thermophysics* **23**, 1207–1216.
- RICHARDSEN, T. & LOHOEFER, G. 1999 Contactless electrical conductivity measurement of electromagnetically levitated metallic melts. *International Journal of Thermophysics* **20**.
- ROLL, A. & MOTZ, H. 2000 *Z. Metallk* **48**, 272–280.
- SCALA, E. & ROBERTSON, W. D. 1953 *Journal Metals Trans* **197**, 1141–1147.
-

REFERENCES

- SEETHARAMAN, S., MCLEAN, A., GUTHRIE, R. & SRIDHAR, S. 2014 *Treatise on Process Metallurgy: Process Fundamentals*. Elsevier Ltd.
- SHARAFAT, S. & GHONIEM, N. 2000 Summary of thermo-physical properties of sn, and compounds of sn-h, sn-o, sn-c, sn-li, and sn-si and comparison of properties of sn, sn-li, li, and pb-li. *University of California Los Angeles* .
- SHERCLIFF, J. A. 1962 *The Theory Of Electromagnetic Flow-Measurement*, 1st edn. Cambridge University Press, Cambridge, 146 pages.
- SIVAK, B. A., GRACHEV, V. G., V. M. PARSHIN, A.D. CHERTOV, ZARUBIN, S. V., FISENKO, V. G. & SOLOVEV, A.A. 2009 Magnetohydrodynamic processes in the electromagnetic mixing of liquid phase in the ingot on continuous bar- and bloom-casting machines. *Steel in Translation* **39**, 774–782.
- TAYLOR, JOHN R. 1997 *An Introduction to Error Analysis: The Study of Uncertainties in Physical Measurements*, 2nd edn. University Science Books.
- THESS, ANDR, VOTYAKOV, EVGENY, KNAEPEN, BERNARD & ZIKANOV, OLEG 2007 Theory of the lorentz force flowmeter. *New Journal of physics* **9** (299).
- THESS, ANDR, VOTYAKOV, EVGENY V. & KOLESNIKOV, YURII 2006 Lorentz force velocimetry. *Physical Review Letters* **96**.
- THOMPSON, WILLIAM J. 1994 *Angular Momentum*. John Wiley and Sons, Inc.
- UHLIG, ROBERT P., ZEC, MLADEN, BRAUER, HARTMUT & THESS, ANDR 2012 Lorentz force eddy current testing: a prototype model. *Journal of Non-destructive Evaluation* .
- WEIDERMANN, C. 2013 Design and laboratory test of a Lorentz force flowmeter for pipe flows. *PhD thesis, Ilmenau University of Technology* .

Acknowledgments

Working on the Ph.D. has been a wonderful and often overwhelming experience. It is difficult to say whether it has been grappling with the topic itself that has been the real learning experience or grappling with how to write papers and reports, give talks, work in a group, stay for long hours in lab also in weekends, and stay focused. In any case, I am indebted to many people for making the time working on my Ph.D. an unforgettable experience.

First and foremost, I am deeply grateful to my advisor, professor André Thess. It has been an honor to be his Ph.D. student. He has taught me, both consciously and unconsciously, how good experimental science is done. I appreciate all his contributions of time, ideas, and encouragement to make my Ph.D. experience productive and stimulating. I am also thankful for the excellent example he has provided as a successful leader and professor.

Furthermore, I am very grateful to my second supervisor, Professor Thomas Fröhlich, who was always there for me. He supported me with his creative ideas whenever I asked him. It was an honor to be a student of such a great professor.

I would like to express my deep appreciation to Prof. Yurii Kolesnikov, who helped, supported, and guided me through my Ph.D. project. The door to his office was always open for me to come and ask any questions. He was my second father in Germany and made me feel home.

I would like to take the opportunity to thank Prof. Donald R. Sadoway at Massachusetts Institute of Technology (MIT) in Cambridge, US, for his warm hospitality in his lab. Working under your supervision and with your creative team was unforgettable.

Acknowledgements

A special thank to Prof. Christian Karcher. Our open mind, open heart discussions helped me a lot to see the world through a different point of view and out of the box. I am very grateful to meet someone like you!

In addition, I have been very privileged to get to know and to collaborate with many other great people who became friends over the last years. I learned a lot from you about life, research, how to tackle new problems, and how to develop techniques to solve them. I am very thankful to Vinodh, Igor, Natascha, Jan, Matthias, Konstantin, Suren, Sebastian, and Judith.

There have been many technical problems that I wouldn't have been able to overcome without the help of Eckhart Roth and Vigimantas Mitscgunas. Thank you very much!

Last but not least, I would like to thank my parents, Fadel Alkhalil and Naam Samaan, my sister, and my brothers for their support. Without your encouragement, this would not have been possible.

I am also grateful to the German Research Foundation (Deutsche Forschungsgemeinschaft) for supporting the work in the framework of the Research Training Group 1567 (Graduiertenkolleg) "Lorentz force velocimetry and Lorentz force eddy current testing" at Ilmenau University of Technology.

Erklärung

(gemäss Anlage 1 der Promotionsordnung der TU Ilmenau - Allgemeine Bestimmungen)

Ich versichere, dass ich die vorliegende Arbeit ohne unzulässige Hilfe Dritter und ohne Benutzung anderer als der angegebenen Hilfsmittel angefertigt habe. Die aus anderen Quellen direkt oder indirekt übernommenen Daten und Konzepte sind unter Angabe der Quelle gekennzeichnet. Bei der Auswahl und Auswertung folgenden Materials haben mir die nachstehend aufgeführten Personen in der jeweils beschriebenen Weise entgeltlich/unentgeltlich geholfen:

- **Prof. Dr. André Thess** (Leiter Fachgebiet des Instituts für Technische Thermodynamik an Deutsches Zentrum für Luft- und Raumfahrt (DLR): Fachliche Betreuung während der Promotionszeit.) → unentgeltlich
- **Prof. Dr. Thomas Fröhlich** (Leiter Fachgebiet Leiter des Instituts für Prozessmess- und Sensortechnik an der Technischen Universität Ilmenau: Fachliche Betreuung während der Promotionszeit.) → unentgeltlich
- **B.Sc. Muhammad Adeel** und **B.Sc. Moustafa Aljarad** (Studentische Hilfskraft an der Technischen Universität Ilmenau: Unterstützung der Messung von elektrischen Leitfähigkeit der Lorentzkraft-Sigmometrie.) → unentgeltlich
- **Editage - English Language Editing Services** (Sprachkorrektur; Ausschliesslich Bearbeitung von Rechtschreibung und Grammatik. Es wurden keine inhaltlichen Änderungen, Ergänzungen oder weitere Beiträge durch die Editoren vorgenommen.) → entgeltlich

Weitere Personen waren an der inhaltlich-materiellen Erstellung der vorliegenden Arbeit nicht beteiligt. Insbesondere habe ich hierfür nicht die entgeltliche Hilfe von Vermittlungs- bzw. Beratungsdiensten (Promotionsberater oder anderer Personen) in Anspruch genommen. Niemand hat von mir unmittelbar oder mittelbar

geldwerte Leistungen für Arbeiten erhalten, die im Zusammenhang mit dem Inhalt der vorgelegten Dissertation stehen.

Die Arbeit wurde bisher weder im In- noch im Ausland in gleicher oder ähnlicher Form einer Prüfungsbehörde vorgelegt.

Ich bin darauf hingewiesen worden, dass die Unrichtigkeit der vorstehenden Erklärung als Täuschungsversuch bewertet wird und gemäss Paragraph 7 Abs. 10 der Promotionsordnung den Abbruch des Promotionsverfahrens zur Folge hat.

Ilmenau, den 27.11.2015

Shatha Alkhalil